In situ Cryocrystallization: Pathways to Study Intermolecular Interactions

Deepak Chopra AND T. N. Guru Row

Abstract | *In situ* crystallization of a liquid, the subsequent determination of its molecular and crystal structure and consequent study of intermolecular interactions is an area of contemporary interest. This technique has been successfully applied for the structure determination of compounds, which are liquids at room temperature, solvents, low-melting solids, gas hydrates and ionic liquids. Particularly in solvents, the importance of how the molecules pack in the crystal lattice is of relevance in the context of polymorphic modifications and their possible implications in directing other molecules to crystallize. *In situ* cryocrystallization, i.e. crystallization of compounds in capillaries on the diffractometer, has offered meaningful outputs to understand both intra- and inter-molecular interactions. These offer well defined targets for molecular design, which can be exploited for the design of futuristic materials including areas like drugs, pharmaceuticals and technologically important materials.

1. Introduction

Any liquid state is a complex dynamic system characterized by a variety of intermolecular interactions responsible for molecular association. The related properties such as solubility and miscibility strongly depend on the strength and directionality of these interactions. The role of strong, weak and van der Waals interactions in generating different supramolecular assemblies is unprecedented and assumes prime importance in the context of crystal engineering. Researchers over the world have used this methodology towards the understanding of related physical properties like viscosity and surface tension, and also to determine the three dimensional structure of natural products.

More intended structure determinations by X-ray diffraction fail nowadays because of the lack of suitable single crystals than for any other reasons. Thus crystallization devices, where we can perform controlled crystallization with simultaneous monitoring of the growth and a check on the quality of the desired single crystals is of importance.

In this review, we explain the methodology in detail, highlighting the work done in several areas of relevance such as ionic liquids, solvents, gas hydrates and low melting solids.

2. Equipment and instrumentation

2.1. *Our instrumentation strategy at IISc*

The Single crystal facility consists of a Bruker APEX CCD diffractometer equipped with OXFORD cryosystem as low temperature attachment. The procedure for collecting data on crystals obtained by solidification of liquid has been optimized. The sample mounting characteristics like diameter of the Lindemann capillary, length and amount of the sample to be taken have been analyzed with greater precision. The procedure for obtaining crystals, in absence of OCHD is very laborious, painstaking, time consuming and the probability of success is very low. In this regard, initial DSC

Solid State and Structural Chemistry Unit, Indian Institute of Science, Bangalore 560012, India
ssctng@sscu.iisc.ernet.in

Figure 1: The CCD facility set up at IISc, Bangalore. The goniometer attachment, capillary head and nitrogen cryosystem are shown.

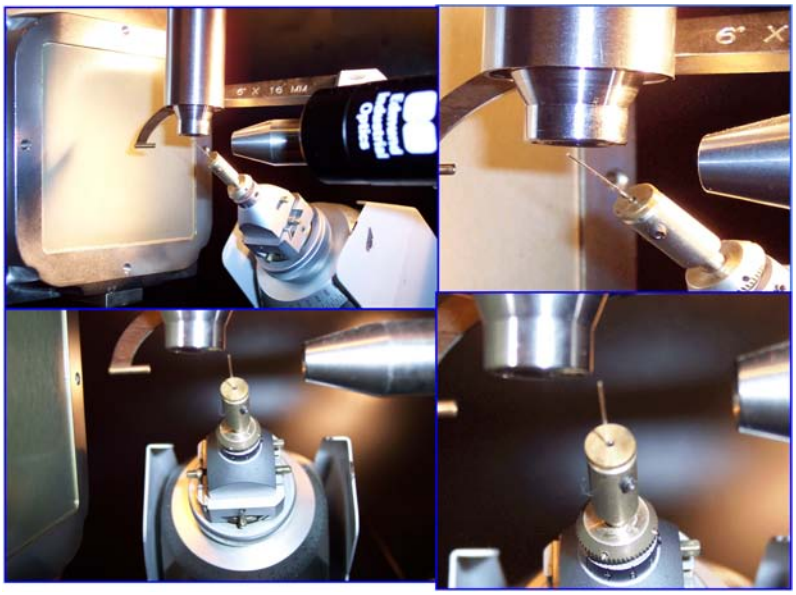

Figure 2: OCHD device (Reproduced by courtesy: Prof. Böese).

data (Differential Scanning Calorimetry) enables one to design the crystallization experiments on the diffractometer. The shape of the DSC curve provides useful information about the crystallizing nature of the sample. The RAMP rate is another important physical parameter, which has been standardized so as to overcome the glass transition temperature and avoid glass formation inside the capillary. After a series of time entailing experiments, appropriate conditions for crystallization of liquid samples in glass capillaries have been obtained.

A Lindemann glass capillary of ~2.5 cm in length and 0.3 mm in diameter was filled with the liquid, sealed by flame on one end and mounted on the Bruker AXS X-ray diffractometer equipped with SMART APEX CCD area detector. Based on the features displayed by Differential Scanning Calorimetry (DSC) analysis, on cooling very slowly at 30 K/h using an OXFORD Nitrogen cryosystem it was observed that complete solidification of the liquid occurred inside the capillary. In the first attempt, with this cooling rate, crystallinity in the sample was ensured by crossing over the glass transition to avoid possible glass formation. In order to obtain a single crystal inside the capillary, a temperature gradient was created by initially moving the nitrogen stream away from the goniometer and after the melting of the solid, the stream was realigned with a time delay. This process of annealing was repeated manually until a well - defined single crystal was obtained. A rotation photograph was taken at this stage to ascertain the quality of the diffraction spots. The temperature was allowed to stabilize for half an hour after which 180 frames of data were collected with the 2θ fixed at $-25°$ and a ω scan width of $-1.0°$. The obtained frames were then processed using SMART and the spots were analyzed using RLATT to determine the unit cell dimensions. Data were collected on three sets of 606 frames with $2\theta = -25°$ and with φ values of 0°, 90° and 180° respectively. The crystal structures were solved using SIR92 and refined in SHELXL97.

2.2. *OHCD—optical heating and crystallization device*

2.2.1. *A system for local heating and in situ crystallization by infrared light in X-ray diffractometry*

Most of the conventional crystallization methods can also be performed in thin Lindeman or quartz capillaries (typical diameter 0.3 mm), which requires a small amount of the sample under investigation. The presence of a low temperature device with every diffractometer makes cooling of neat liquid samples or saturated solutions feasible. However, crystallization by cooling results in formation of a polycrystalline material because nucleation occurs at lower temperatures than the melting point of the neat sample or the saturation point of a solution. Hence local heating is required to produce a molten zone or a temperature gradient within a solution. Any method for local heating will disturb the cold gas stream of the low temperature device and cause icing except heating with an IR-source. Also, by any other external heaters there is the risk to destroy the capillary, obscure the critical range where crystallization takes place and most important, will warm up the cold gas stream so

Figure 3: Trends in the Melting Points and densities of the *n*-alkanes with increasing number of carbon atoms.

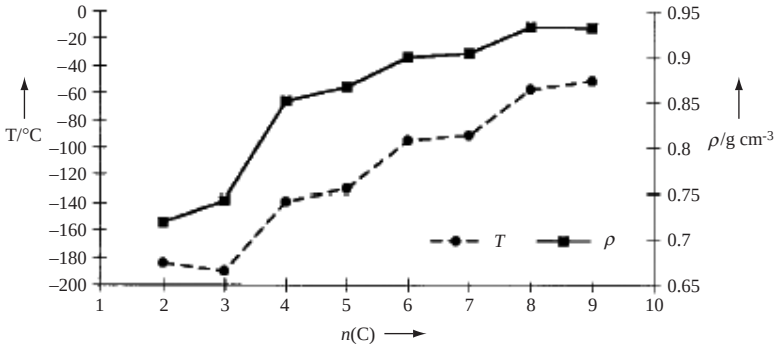

Figure 4: Packing of (a) *n*-hexane and of (b) *n*-heptane viewed along *a* axis.

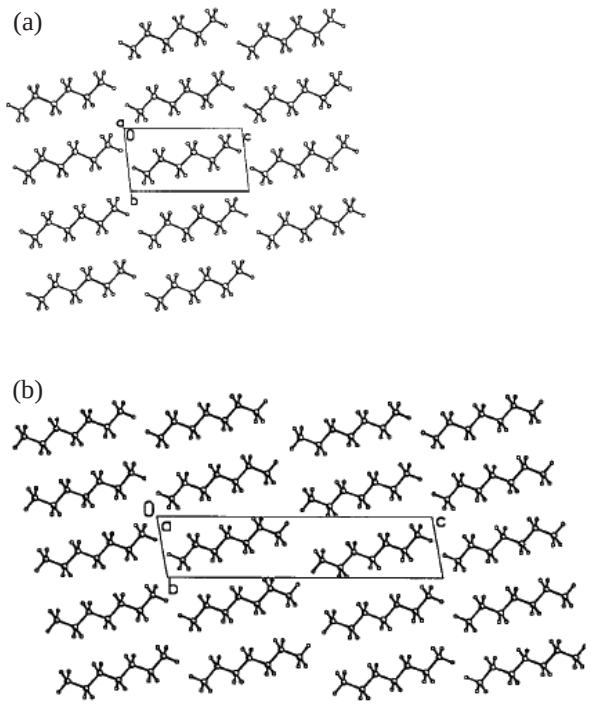

the sample below the heating zone is also warmed and will stay molten. This makes the IR-heating of the capillary superior to other methods. If a focused IR-laser is applied as a heat source, the molten zone (or the clear solvent) can be kept very small (up to 0.1 mm) which also allows to grow crystals moving against the direction of the cold gas stream, which runs usually top to bottom. Bubbles, which often form at the boundary between the solid and liquid phase can be shifted upwards to keep the crystallization zone below undistorted to form a single crystal. The fine focus of the laser also allows for local heating to destroy unwanted satellites with an exact tuning of its position. The IR laser can provide a high temperature gradient for application of a zone refining in order to purify the sample with repeated scans along the capillary, it also allows to sublime samples into the tip of the capillary at very low temperatures. On the other hand, the high stability of the 25 W, water-cooled laser allows a fine dosage of its intensity that is necessary for slow crystallization close to the melting or saturation

Figure 5: Alteration in the melting points and densities in diols (circles) and diamines (squares) with increasing number of carbon atoms.

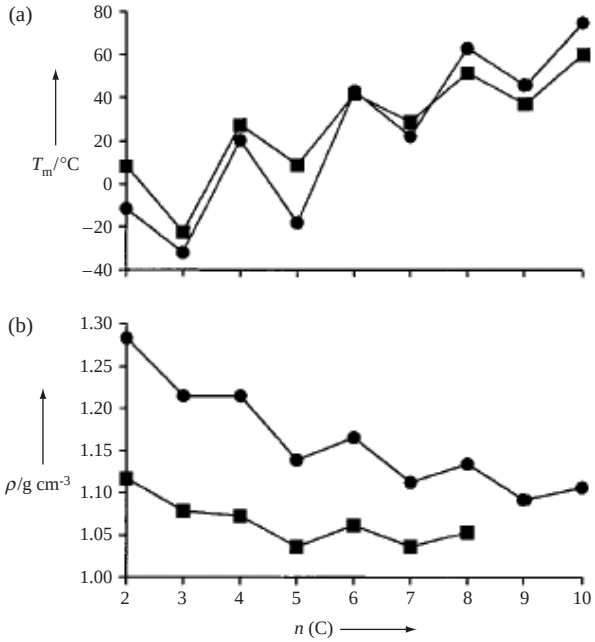

Figure 6: Crystal Structure of 1,7-heptane diol illustrating the three dimensional network of O–H. . . O hydrogen bonds in odd diols.

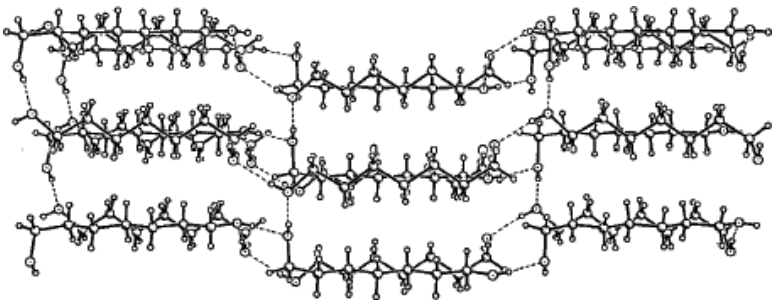

point. Once the optimal crystallization conditions were found by various test runs or manually during the day (crystallization speed and temperature gradient), automated cycles overnight will often produce suitable single crystals. Gradually switching off the laser at an end-position and heating up gradually at a start-position is advised in order to avoid strain in the crystal. Also the start position should be shifted with each cycle so an increasing crystal at the start will remain. Disordered or even plastic phases can be circumvented by crystallization with a high temperature gradient from the neat or in solution. Defocusing the laser will serve as a high temperature source, also applicable for the investigation of high temperature phases or topochemical reactions. For powder diffraction experiments, extreme local heating with the IR laser system is also possible. The small focus of the full power of the 25 W laser can be directed to specific locations of a specimen that are simultaneously shined with the X-ray beam. The local temperature exceeds 1000 °C, of course calibration with samples of known transition points or with commercial available IR-detectors should be performed if the information of the local temperature is really needed. Together with specially designed software

Figure 7: Layered structure in even diols illustrated with the structure of 1,6-hexanediol.

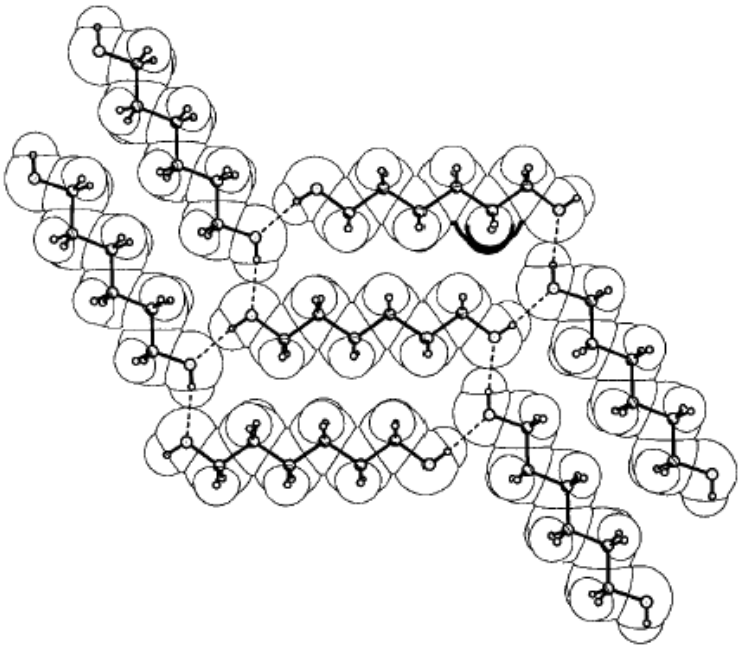

Figure 8: Layered structure in even amines illustrated with the structure of 1,6-hexanediamine.

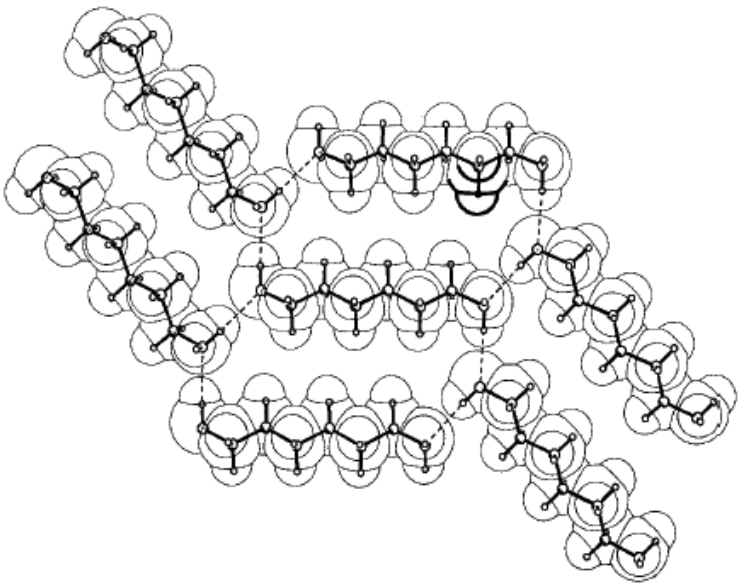

control the **OHCD**[1] provides a system, which makes many experiments feasible, ranging from controlled crystallization to high temperature applications for single crystal and powder diffraction techniques. It consists of a remote, adjustable heat source with a pilot laser, fine controlling of the intensity and one-dimensional position control, adaptable for almost any diffractometer system. The **OHCD** system is currently designed for a Bruker-SMART system with a three-axes platform but can be adapted to almost any diffractometer, with details of the geometric requirements given.

Figure 9: Layer structure in 1,6-hexanedithiol.

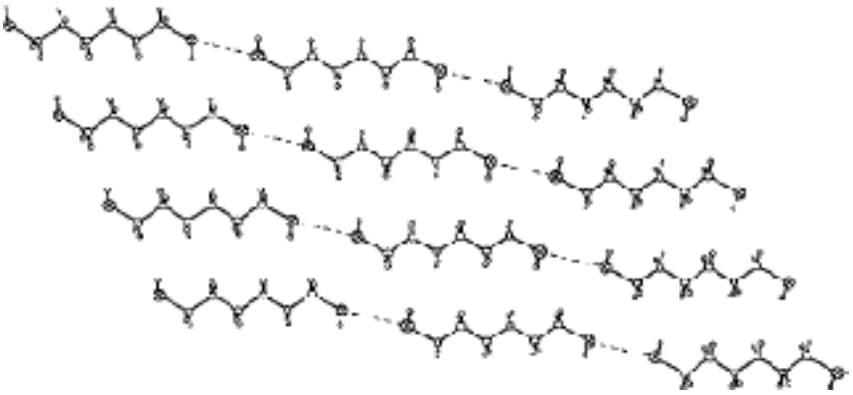

Figure 10: Melting point and Density alteration in diacids.

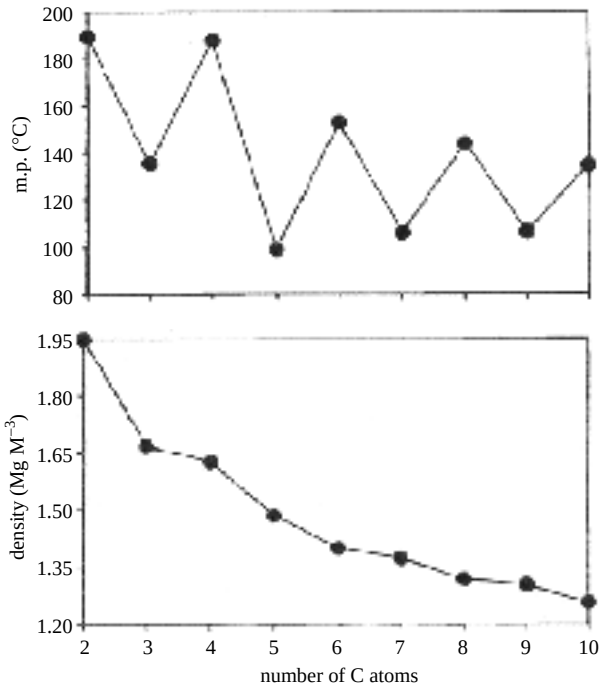

3. Application of the methodology: examples

3.1. *Early results: molecular dimensions and crystal structure of DMSO at* $-60°C$

Work on *in-situ* cryocrystallization started in India in 1966 when Prof M. A. Vishwamitra and Dr K. K. Kannan made attempts to determine the crystal structure of dimethyl sulfoxide[2]. This work is of historical importance as it indictates that the first experiments on cryocrystallization were peformed in our country.

DIMETHYL sulphoxide (DMSO) has been much discussed and investigated in recent years because of its remarkable properties in medicine and as a solvent. The researchers were able to determine the molecular dimensions and crystal structure, at –60°C, from an analysis of three-dimensional X-ray diffraction data. The sample, being a liquid at room temperature, was enclosed and sealed inside a Lindemann glass capillary of 0.3 mm diameter. It was crystallized, *in situ*, inside a low-temperature Weissenberg camera[2]

Figure 11: Layer Structure in C8-diacid. Molecules lie on inversion centers with an all-trans conformation. Lateral molecules are linked through carboxy dimers to form infinite hydrogen bonded chains.

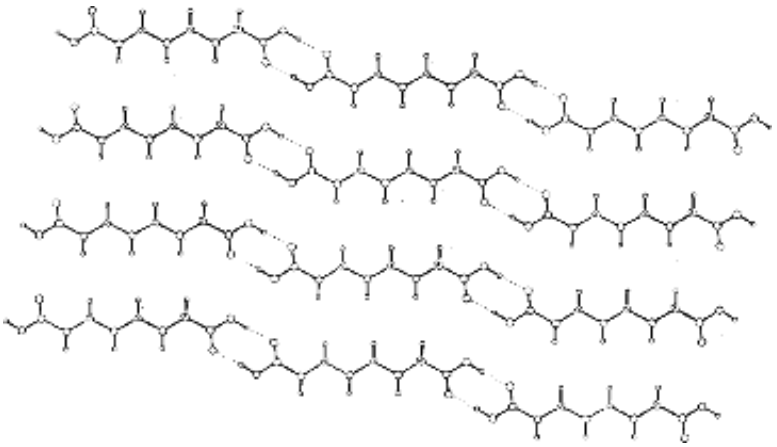

Figure 12: Melting point and crystal density at 180 K for the co-crystals C1–C13.

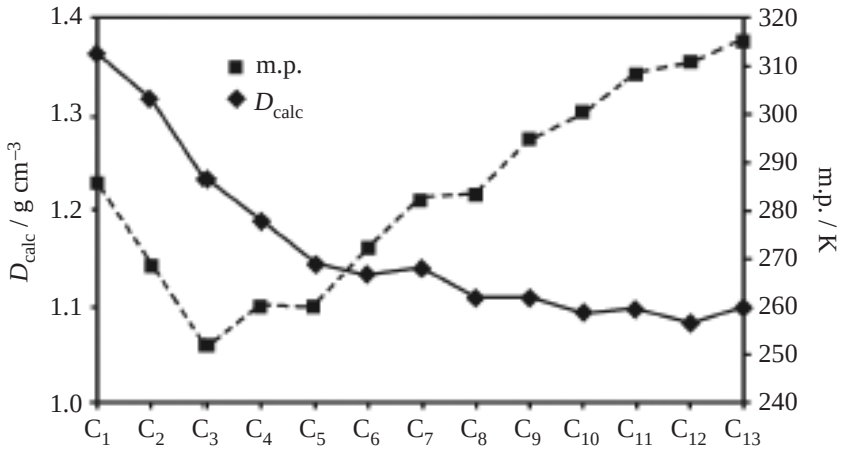

Figure 13: Trimeric units (2:1) carboxylic acid linked via $R_2^2(7)$ O–H. . . N hydrogen bonds.

by slow freezing, melting and refreezing with a jet of cold gas obtained by boiling liquid oxygen[3]. The to-and-fro horizontal movement of the crystal goniometer shaft, involved in this process, was made sufficiently slow and mechanical by coupling the shaft to the spindle of the camera motor by suitable reduction gears. Crossed polaroids mounted on the camera base were used to ensure the quality

Figure 14: Sections through the structures of (a) the even co-crystals (C8 shown) and (b) the odd co-crystals (C7 shown). Shaded regions denote the methyl-group interface and the area A_{Me} denotes the repeating unit within these regions. The third dimension (perpendicular to the planes shown) is comparable in both the odd and even structures.

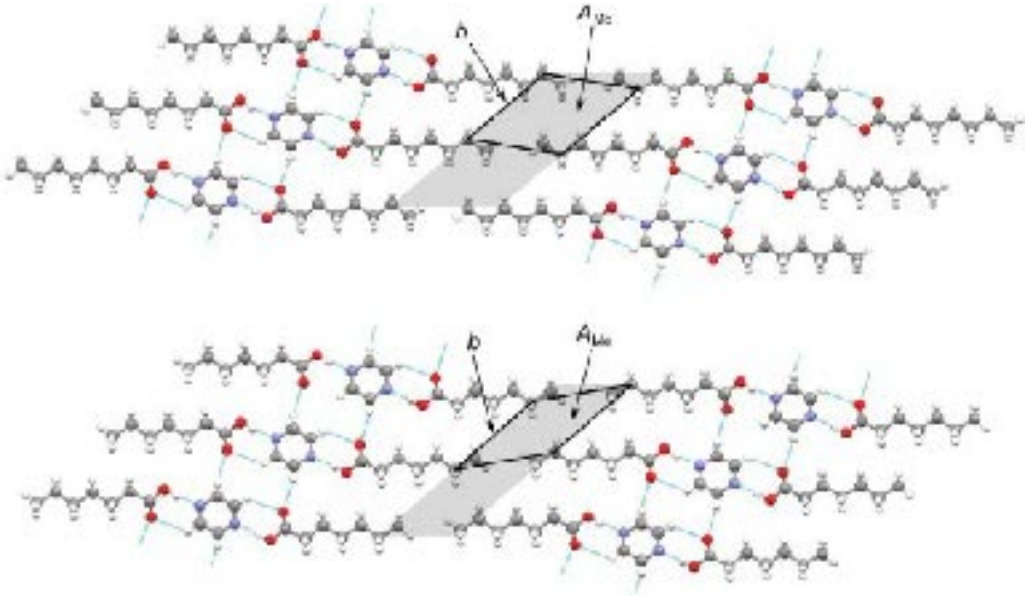

Figure 15: Hydrogen bond scheme of the reference ammonia molecule in the crystal.

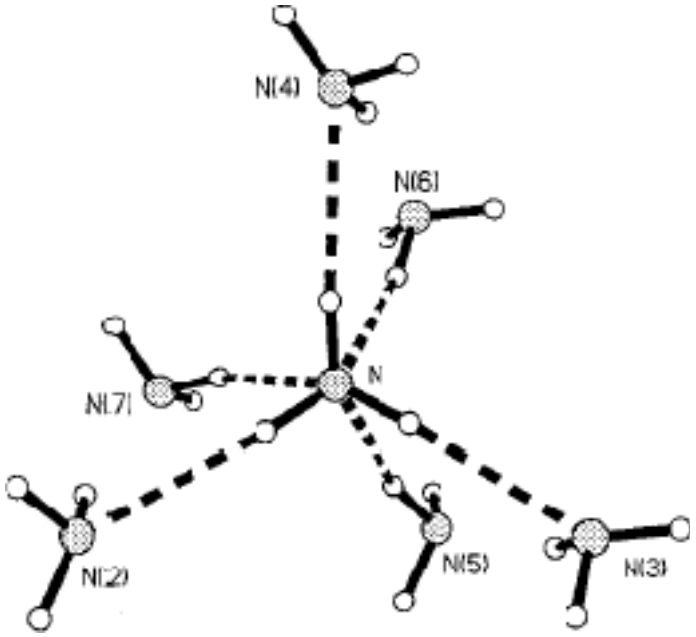

of the crystal, before single-crystal X-ray pictures were taken. Using copper K_α radiation, rotation and $hkL(L = 0, 1, 2, 3)$ equi-inclination intensity data (on multiple films) were collected.

3.2. *Melting point alteration in n-alkanes and unsaturated hydrocarbons*

The melting point alternation in *n*-alkanes and most end-substituted *n*-alkanes has been known for

Figure 16: Dynamic electron density in the crystal of ammonia showing the formation of hydrogen bond in the plane of the reference atom of the N(7)-H bond of neighbouring molecule.

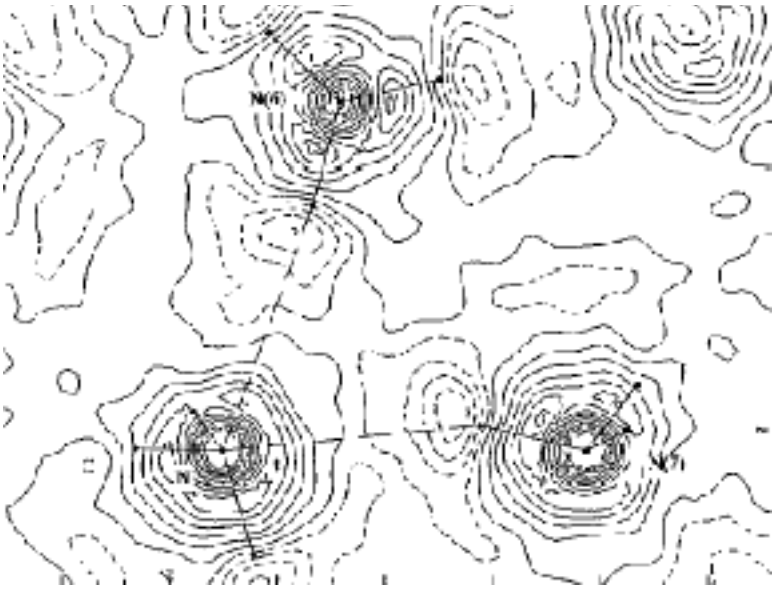

Figure 17: Dynamic electron density of the ammonia molecule in the planes normal to the 3-fold axis and passing through the nitrogen atom lone pair.

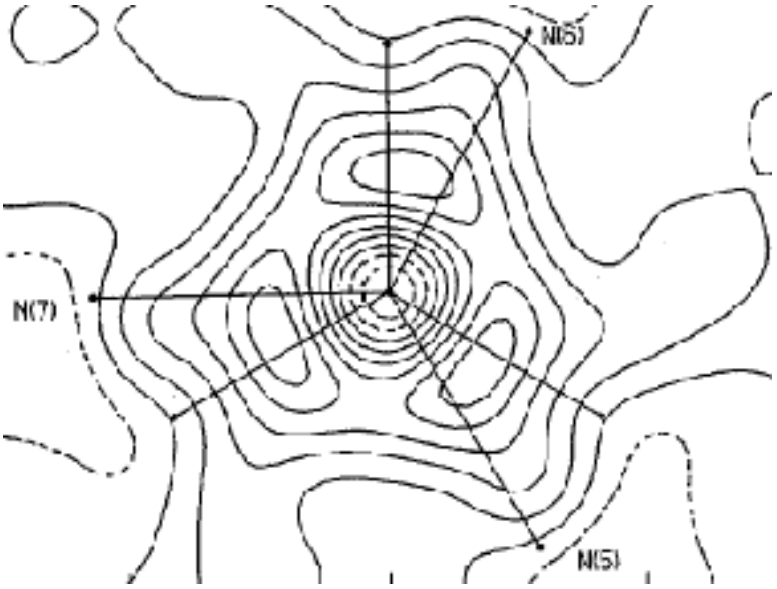

decades. Physical properties such as solubilities and sublimation enthalpies that are related to the solid state also exhibit an alternating pattern, whereas those related to the liquid state show monotonic behavior. *n*-alkanes are solely held together by hydrophobic interactions in the solid state, Boese *et al.*, have shown recently that the melting point alternation (Figure 3) in *n*-alkanes[4] can be explained in terms of a simple geometrical model.

Ethane, propane and butane form layer structures in the solid state. By describing their molecular geometries as a rectangle, irregular

Figure 18: General view of the molecular structure of II in two projections and atom numbering scheme: (a) "side on" view (b) view from the "top".

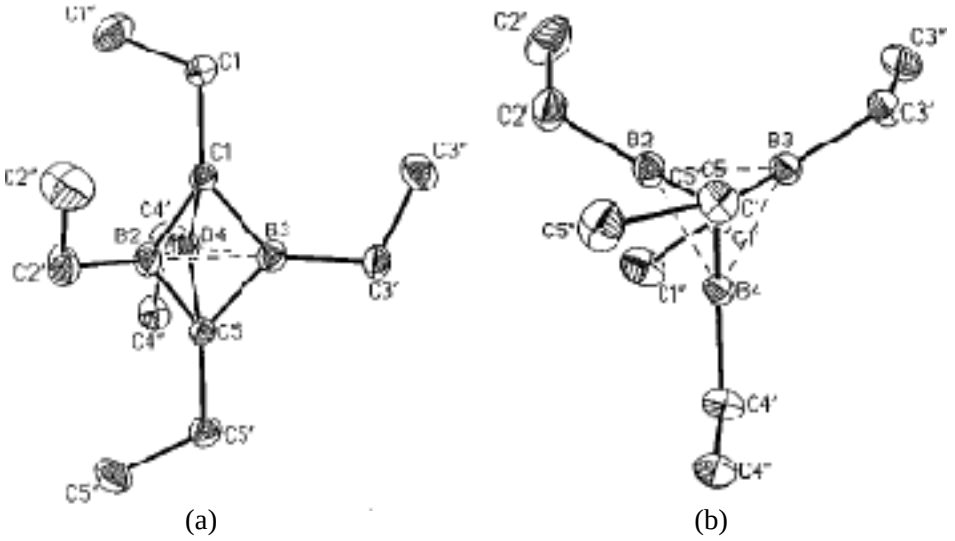

Figure 19: Dynamic electron density in the equatorial B-B-B plane.

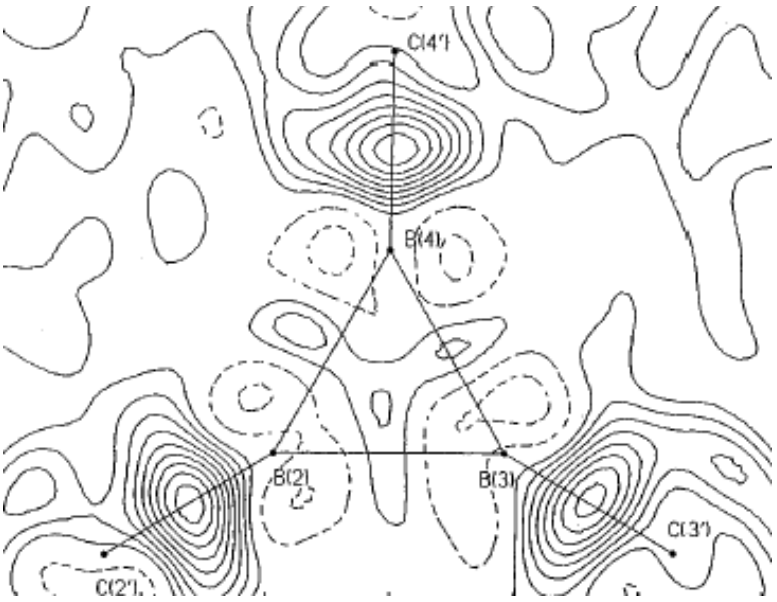

pentagon and irregular hexagon respectively it is shown that propane cannot close-pack like its congeners and hence the melting point of propane is lower than expected. In the series from *n*-hexane to *n*-nonane crystallize in triclinic P-1 crystal system with the lengths of *a* and *b* axis remaining similar with increasing chain length. The crystal packing in hexane and heptane is as shown in Figure 4. The methylene groups fit into the hollows of the neighbouring chains, which cause a shift along the *c*-axis. The packing of the molecules along the *c*-axis leads to differences in the cell volumes and densities and the lateral packing does not play any role in the observed differences in densities. The methyl groups at the end of the chain adopt a staggered conformation. The even numbered alkanes have optimal intermolecular contacts at both ends whereas the odd ones possess these at

Figure 20: Laplacian plot of the molecule in the axial plane.

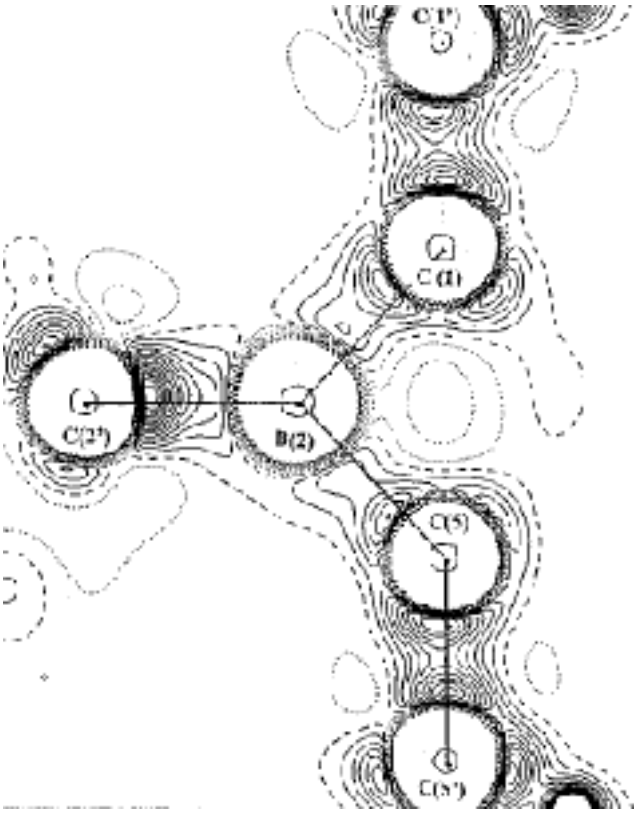

one end and at the other end the distances are longer. This leads to less dense packing for the odd *n*-alkanes and as a consequence resulting in lower melting points.

Following, this work on saturated hydrocarbons, Bond *et al*., determined the low temperature crystal structures of 1,7-octadiene (C_8H_{14}), 1,9-decadiene ($C_{10}H_{18}$), 1,7-octadiene (C_8H_{10}, 1,9-decadiene ($C_{10}H_{14}$),[5] following *in-situ* crystal growth from liquid. The study reveals the importance of C–H...π interactions in organizing molecules in the solid state. The low temperature crystal structure of ethene and ethyne also contains networks of C-H...π interactions at near-linear geometry.

3.3. *Melting point alteration in α, ω-alkanediols and α, ω-diamines*

Boese *et al*., have undertaken a structural study of the diols $HO(CH2)_nOH$ ($n = 2$–10) and the diamines $H_2N(CH_2)_nNH_2$ ($n = 2$–8)[6] in order to correlate packing densities with the observed alteration in melting point behaviour (Figure 5). Most of these are liquids at room temperature, and their single crystals have been grown *in situ* using a miniature zone melting procedure with an IR laser. The melting points were recorded by differential scanning calorimetry and no indications of phase transitions were found.

The analysis of the crystal structures of diols and diamines has revealed the interplay between two important intermolecular interactions that are possible in these amphiphilic compounds, namely, hydrogen bonding and hydrophobic interactions (Figures 6–8). While hydrogen bonding and hydrophobic interactions operate in consonance in even members, and therefore culminate in dense packing, they run into geometrical conflicts in odd members, leading to looser packing. Accordingly, the odd members of the diol and diamine series have relatively lower densities and melting points than the even members. The even membered compounds pack in a layered structure whereas the odd membered compounds in a three dimensional structure.

The end groups in diols and diamines are involved in the formation of hydrogen bonds, namely O–H...O and N–H...N respectively, and the alkyl chains participate in van der Waals interactions. While hydrogen bonding energies are similar it is the differences in hydrophobic interactions, which is responsible for the observed differences in packing densities.

Figure 21: Molecular structure of acetylacetone (AA) at 110 K with the atom numbering scheme drawn with 50% ellipsoidal probability.

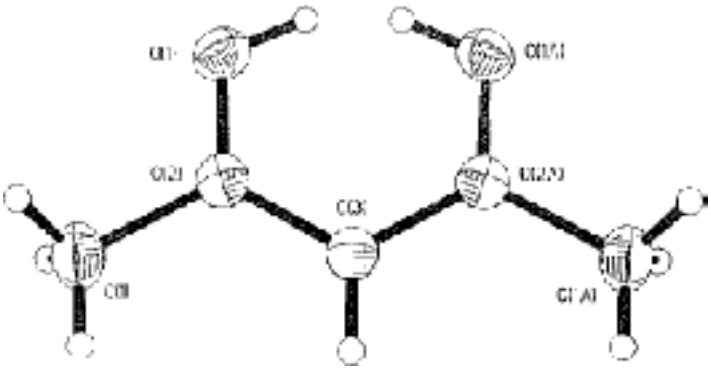

Figure 22: Dynamic electron deformation density in the molecular plane of AA.

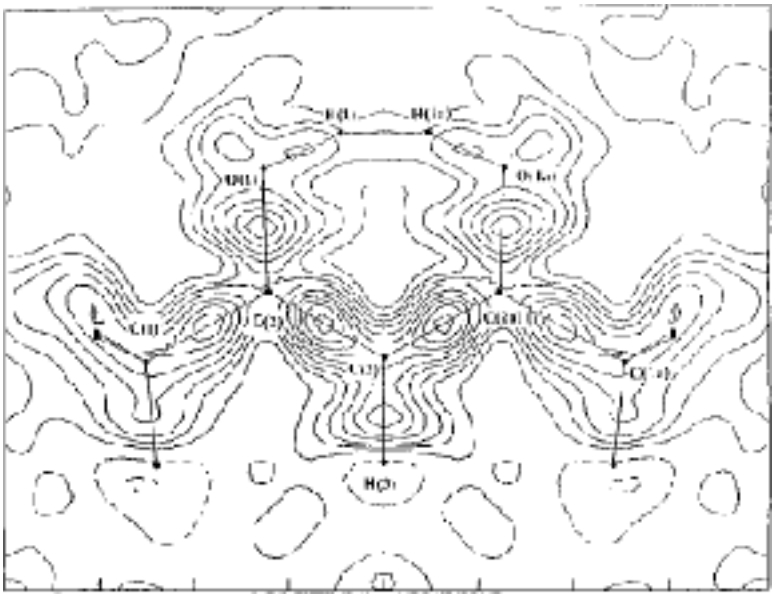

3.4. *Melting point alteration in α, ω-alkanedi-thiols*

R-Alkanedithiols show an alternation in their melting points with even members exhibiting systematically higher melting points than odd members. In this study, single crystals of the first nine members of *R*-alkanedithiols (HS–$(CH_2)n$–SH, $n = 2$–10) have been grown *in situ* using a miniature zone melting procedure[7], and their X-ray analyses have been performed. The structural similarities and differences between even and odd members have been analyzed based on the packing arrangements of hydrocarbon chains and SH functionalities. Whereas the hydrocarbon chains maintain an intergrooving pattern, the SH groups associate in an anti-parallel fashion in both the members (Figure 9). The SH groups do not form hydrogen bonds. In the even members the molecules are offset along their length, whereas such an offset is not observed in the odd members. The densities of even members are systematically higher than those of odd members and show an alternating trend. Using a simple geometrical model, describing even and odd members as modified parallelograms and trapezoids, respectively, the density features of the packing patterns in both the members are illustrated. The melting point alternation in dithiols is attributed to the geometry allowed or forbidden molecular offset toward a higher packing density.

Figure 23: (a): ORTEP of [emim]BF_4 drawn with 50% ellipsoidal probability. (b): ORTEP of [bmim]PF_6 drawn with 50% ellipsoidal probability. (c): ORTEP of [bmim]OTf drawn with 50% ellipsoidal probability. (d): ORTEP of [hexpy]NTf_2 drawn with 50% ellipsoidal probability. (e): ORTEP of [bmpyr]NTf_2 drawn with 50% ellipsoidal probability. (f): ORTEP of [emim]OTf drawn with 50% ellipsoidal probability. (g): ORTEP of [emim]NTf_2drawn with 50% ellipsoidal probability.

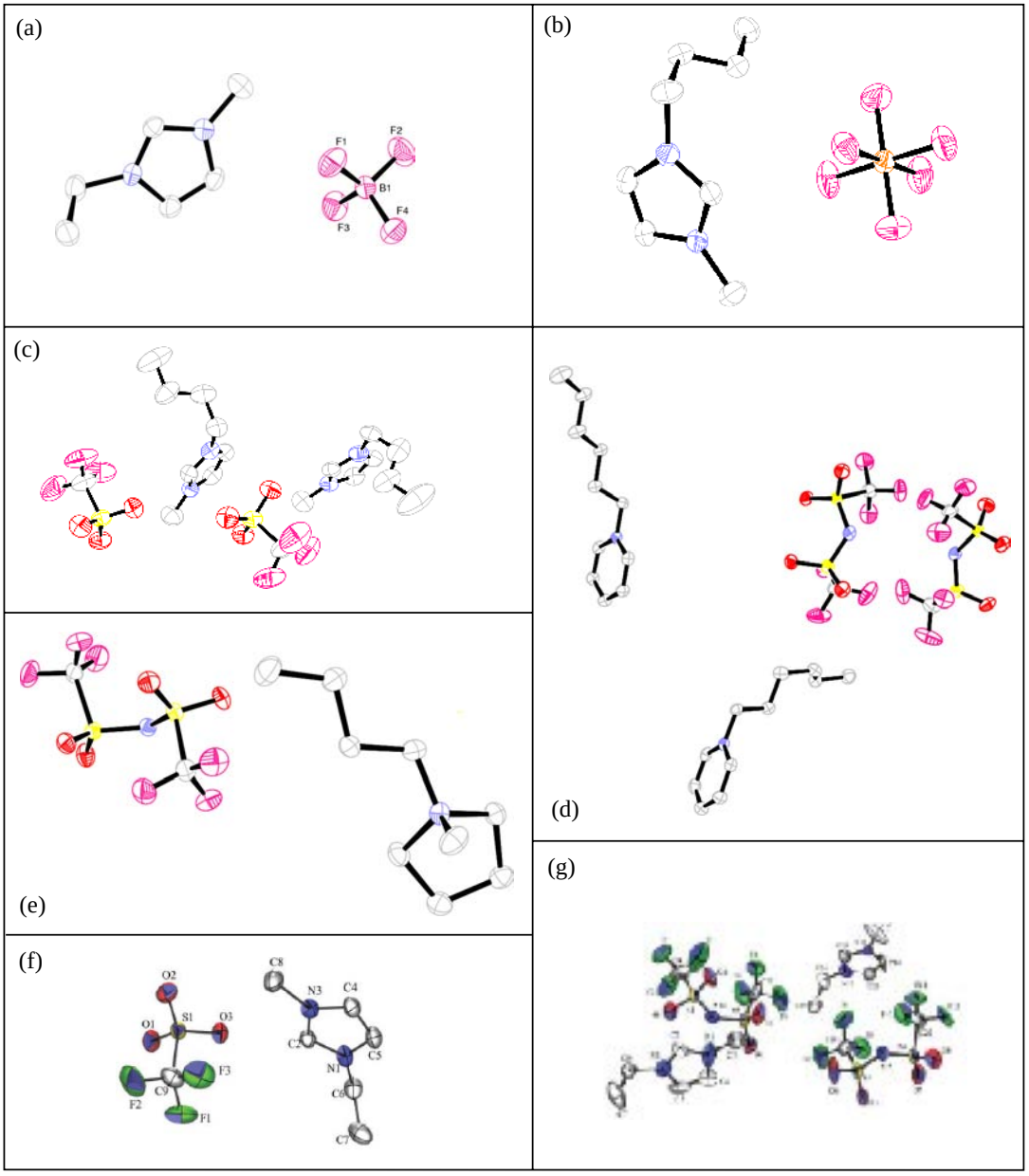

3.5. *Melting point alteration in α, ω- alkanedicarboxylic acids*

Single crystal studies on α, ω- alkanedicarboxylic acids have been performed. The melting points show alteration (Figure 10) with members containing an even number of carbon atoms exhibiting systematically higher melting points compared to odd ones. On the contrary the solid-state densities of odd members with $C_n \geq 5$ are higher than those of even members. Close packing principles are not responsible for alternating melting point in diacids. The structural features in both even and odd di-acids exhibit packing regularities. The carboxy groups form hydrogen-bonded dimers at both ends of the molecules, leading to infinite chains and methylene groups stack into columns through van der Waals interactions (Figure 11). In the context of melting point measurements there exists

Figure 24: Crystals of the polymorphic forms of diphenyl ether grown insitu in the capillary.

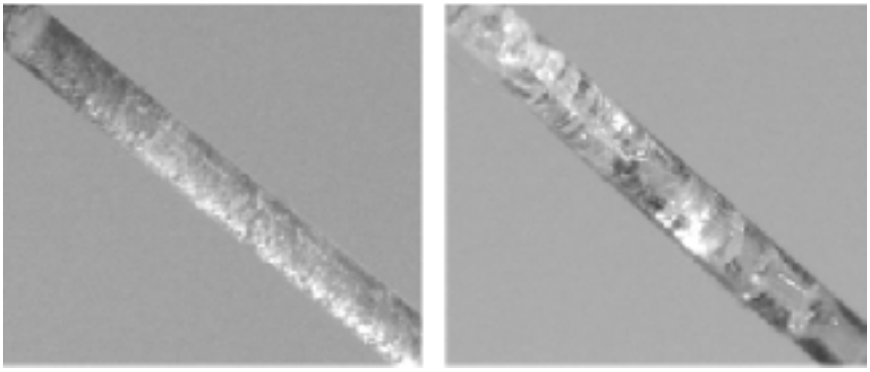

Figure 25: ORTEPs of Form I and II of diphenyl ether, drawn with 50% ellipsoid probability.

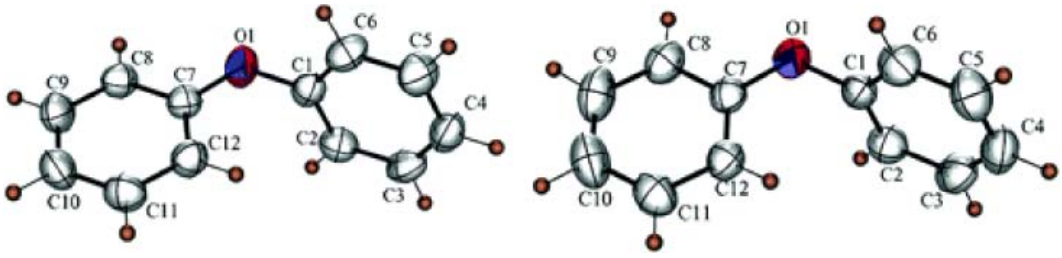

Figure 26: Packing of molecules of diphenyl ether in form I. (b) Packing of molecules of diphenyl ether in form II.

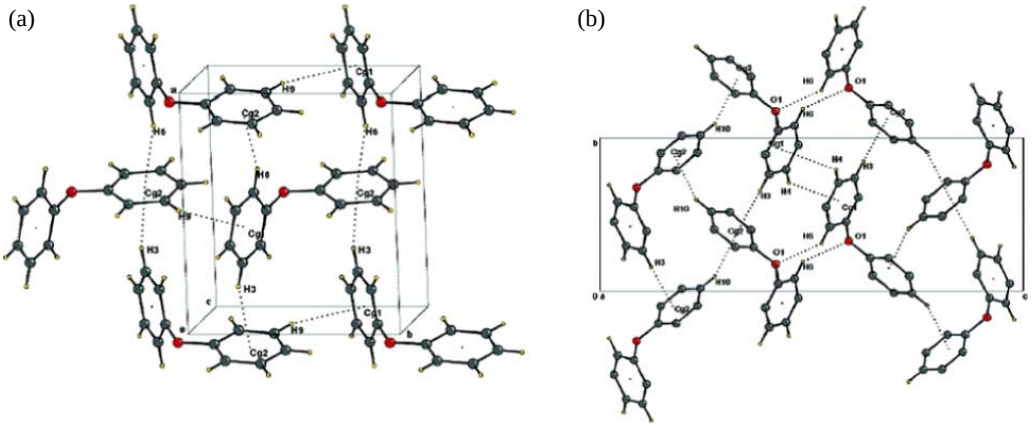

certain differences in packing patterns. Molecules are offset along their length within the columnar stacks in even members, whereas such an offset is absent in odd members and molecules in odd members exhibit twisted molecular conformation as opposed to non-twisted all-*trans* conformation in the even members. A simple geometrical model has been developed wherein the even and odd members are described as modified paralleleograms and trapezoids respectively. The packing of paralleleograms allows an offset, which reduces repulsion between the carboxy dimers

Figure 27: Cage shapes in the clathrates. From left to right, top row: dodecahedron, tetrakaidecahedron, hexadecahedron; bottom row: irregular dodecahedron and icosahedron.

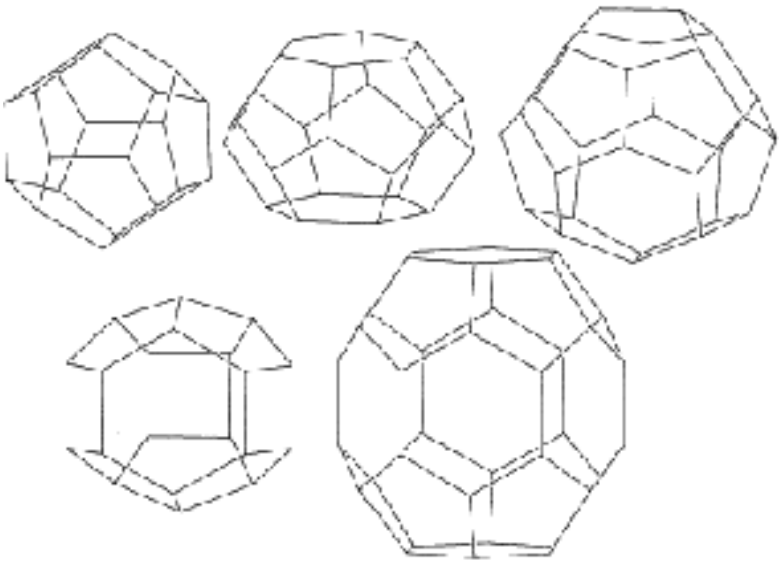

Figure 28: Packing of SI gas hydrate. The outlined dodecahedron is surrounded by eight tetrakaidecahedra.

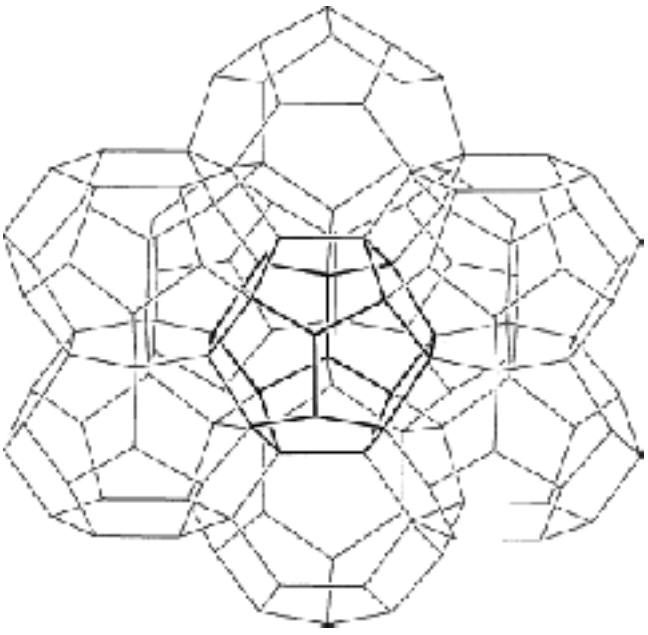

of adjacent hydrogen-bonded chains whereas in trapezoids a similar offset is forbidden. Thus the melting point alteration in diacids is therefore attributed to the geometry allowed or forbidden attainment of offset packing with a non-twist molecular conformation.

3.6. *Melting point alteration in cocrystals of pyrazine and n-alkyl carboxylic acids*

The crystallization of binary compounds, which are liquids at room temperature, has been attempted and structures of 2:1 cocrystals of the *n*-alkylcarboxylic acids with pyrazine[9] have

Figure 29: Packing of structure II gas hydrate. The hexakaidecahedra of tetrahedral symmetry form a diamondal network of which a six-membered ring is shown. The dodecahedra fill the voids within this network.

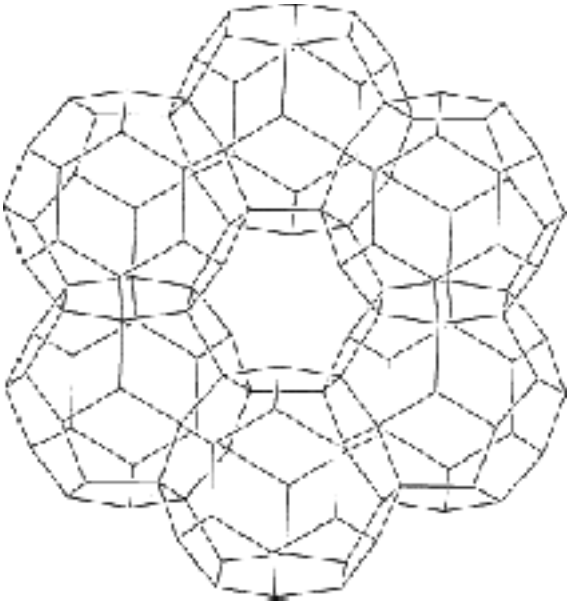

Figure 30: Structure of gas H hydrate. A central icosahedron is surrounded by six irregular dodecahedra.

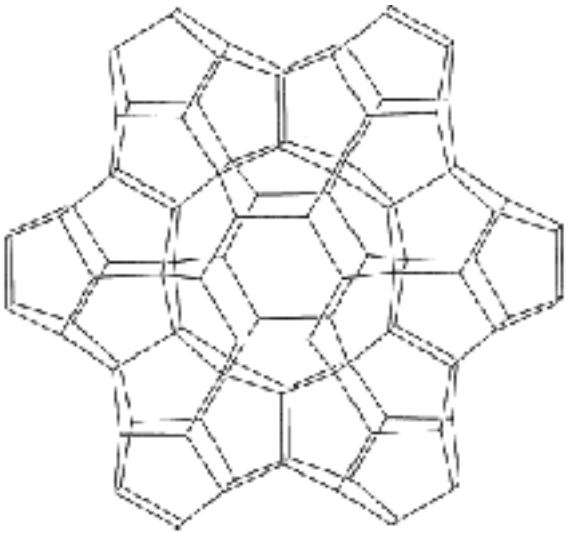

been determined (denoted by C_1– C_{10}). The series has been extended further to include C_{13}. From methanoic acid to tridecanoic acid, the cocrystal structures exhibit considerable variation. For heptanoic acid and longer acids, the structures display regularities and the structures display an alteration in their melting points that is opposite to that in *n*-alkylcarboxylic acids themselves, the melting points of the odd co-crystals are systematically higher than those of the evens members (Figure 12). The melting points are directly correlated with the crystal density, which is systematically lower in the even co-crystals on account of reduced packing efficiency at the methyl group interface between layers in the structures. The arrangement of the methyl groups is governed by a

Figure 31: Cocrystal of acetylene:acetone 1:2 viewed down the (100) plane.

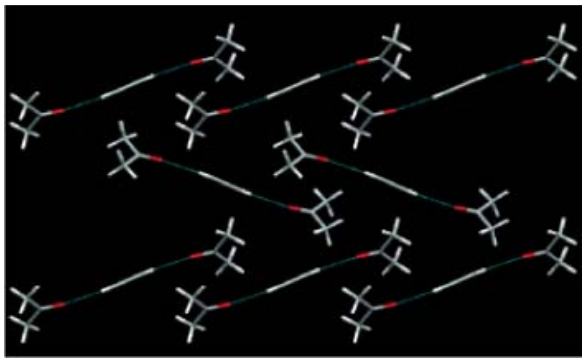

Figure 32: Cocrystal of acetylene:acetone 1:1 viewed down the (100) plane.

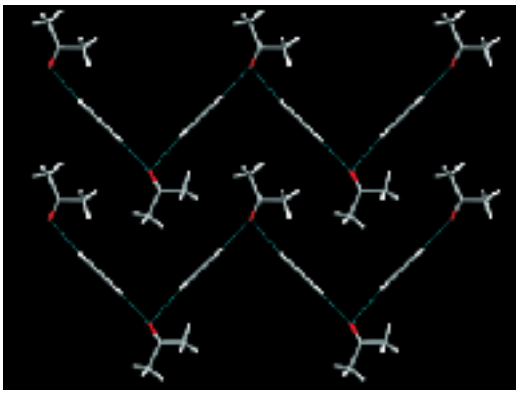

consistent arrangement of pyrazine moieties within the layers.

In each of the co-crystal structures, molecules are linked into trimeric (2:1) units via $R_2^2(7)$ motifs, in which an O–H…N hydrogen bond between the carboxylic acid and pyrazine moieties is supported by a coplanar C–H…O interaction (Figure 13).

The manner in which these trimeric units are arranged is variable in the structures of C1–C6, although one common feature is maintained; the long C–H bonds of the pyrazine ring are always directed towards the oxygen atom of the carboxyl group that is not involved in O–H…N hydrogen bond formation. The arrangement in the co-crystals is a consequence of the relative disposition of the pyrazine moieties within each layer, which is essentially indistinguishable within each structure so that the packing density within layers is comparable in each case. This is reflected

Figure 33: Cocrystal of acetylene:acetone 2:1 viewed down the (101) plane. Methyl hydrogens have bee omitted for clarity.

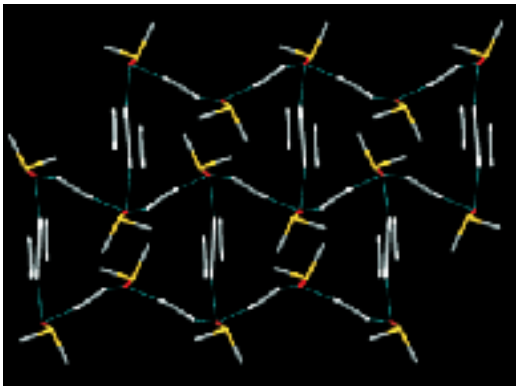

in the minimal variation of the lattice parameter a, b and γ throughout the series. Thus the key difference between the odd and even structures lies in the nature of interactions across the methyl-group interface between layers. Although the arrangement of pyrazine rings is identical in both the odd and even co-crystals, it is the differing orientations of the terminal ethyl groups in the n-alkyl chains that are responsible for the alteration in melting points. In the even structures the terminal bond lie parallel to O–H…N hydrogen bond and form relatively large angles to the methyl group interface. However, in the odd structures, these bonds lie at 109.5° to these hydrogen bonds and form much shallower angles at the methyl group interface. As a result, the packing efficiency between layers is systematically less in the even co-crystals. From simple geometrical considerations, the area of the repeating unit that describes the packing across the methyl group interface (A_{Me}) may be defined as the b dimension of the unit cell multiplied by the perpendicular separation between adjacent lines passing through the methylene units in the ethyl groups (Figure 14). The b dimension differs minimally across the series, but the perpendicular variation is systematically greater in the even co-crystals compared to the odd ones. Hence reduced packing efficiency across the methyl group interface in the even co-crystals leads to a reduced crystal density and hence a decreased van der Waals contribution to the lattice energy.

3.7. *Structure determination of ammonia*

A single-crystal of ammonia, NH_3, was grown in a thin-walled capillary at 178 K, and high-resolution X-ray diffraction data were obtained for this compound at 160 K in order to obtain information about electron density distribution[10]. Conventional

Figure 34: Perspective view of the ClF molecule with two rows of molecules shown along the screw axis.

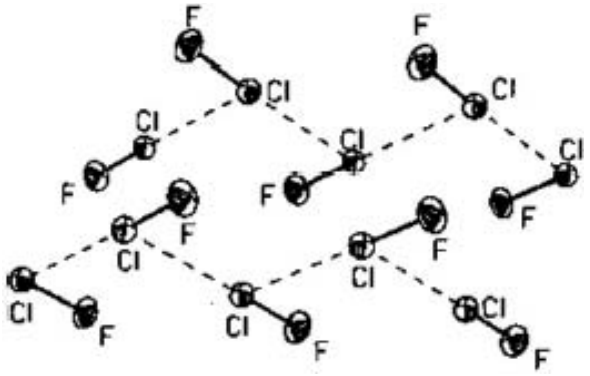

Figure 35: Laplacian of the electron density showing three ClF molecules.

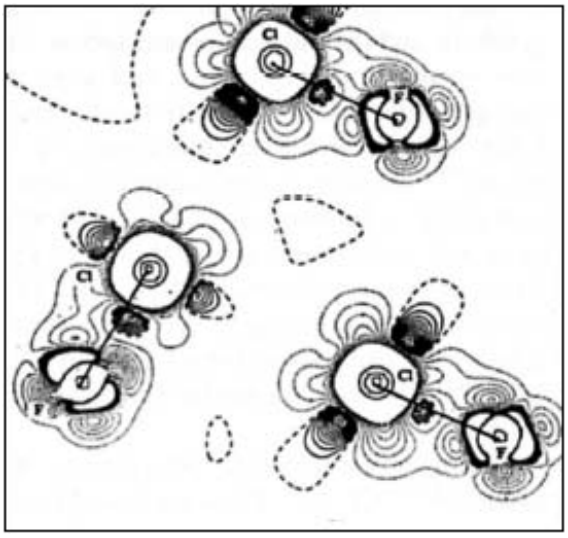

followed by multipole refinements and deformation electron density maps indicated small but significant N–H bond bending inside the NH_3 tetrahedron that is in agreement with *ab initio* quantum chemical calculations and the VSEPR model. Topological analysis of the experimental charge density distribution in the ammonia molecule has been performed, and the data are compared with high-level quantum chemical calculations. Some features of the intermolecular hydrogen bonds in the crystal are discussed.

Ammonia crystallizes in the cubic space group $P2_13$ at 160 K with $a = 5.1305(8)$ Å, $Z = 4$, $V = 135$ Å^3, Density $= 0.838$ gcm^{-3} (Figure 15). On performing a multipolar analysis on the high-resolution charge density data, the electron density distribution and the associated topological properties were obtained using the XD package. After a successful modeling of the electron density, a static deformation density map was plotted depicting the topological properties in ammonia is highlighted (Figure 16–17).

Molecular geometry. Present X-ray data showed the H–N–H angle in ammonia to be 109.0(2)° and N–H bond length to be 0.838(3) Å that is quite normal taking into account that X-ray data usually give shorter X–H bond lengths. Bond angle H–N–H is close to the tetrahedral one and corresponds to sp^3 hybridization of the nitrogen atom. We may compare this angle with the values of 107.2° and 106.7° in the gas-phase studies of ammonia. Neutron powder diffraction data at 180 and 2 K gave bond angles at the nitrogen atom equal to 107.8(4)° and 107.5(2)°. Analysis of all the available data makes it

Figure 36: Unit cell of 1,1,4,4-Tetrafluorobutadiene. Dotted lines indicate intermolecular C–H. . . F interactions.

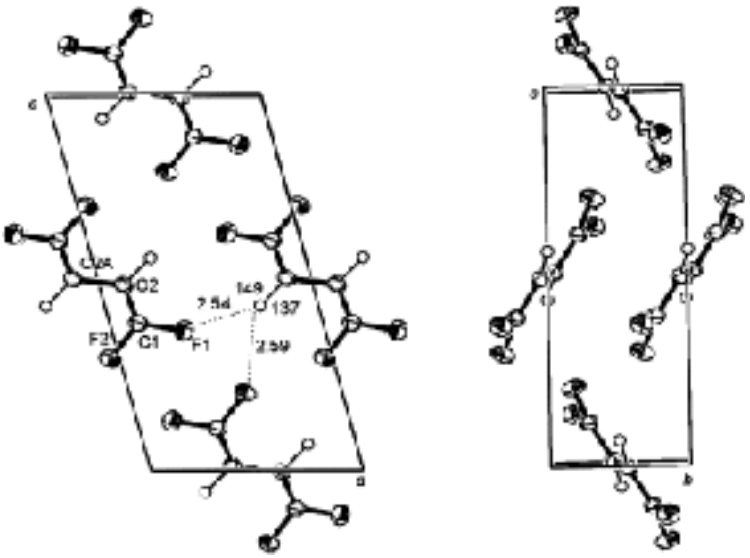

Figure 37: Unit cell of 1,1,4,4-Tetrafluorobutatriene.

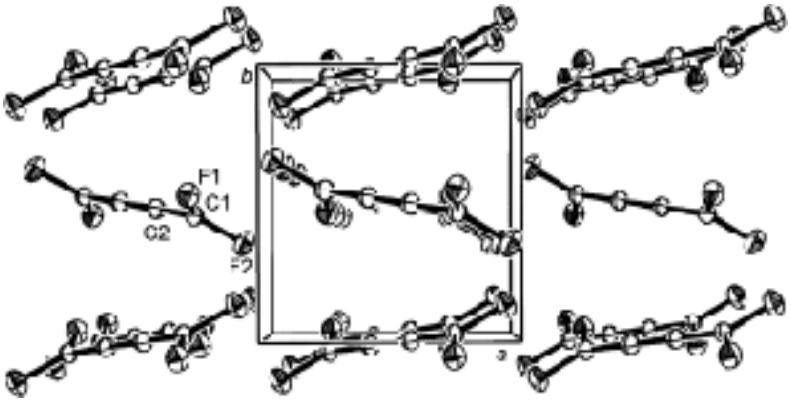

now impossible to make definite conclusions about changes in the molecular geometry of ammonia in free state and in the gas phase. Nevertheless, modern *ab initio* calculations show that the bond angle at the nitrogen atom in ammonia is 1–2° smaller than in the crystal.

3.8. *Boranes electron density distribution*

The molecular and crystal structure and electron density distribution were studied for a single crystal of pentaethyl-1, 5-dicarba-*closo*-pentaborane $C_2B_3(Et)_5$ using high-resolution X-ray diffraction data (Figure 18) at 120 K (5696 observed reflections, $R = 0.056$). The title compound at ordinary conditions represents a low-melting colorless liquid. The single crystal was grown by *in situ* crystallization with an IR-laser beam producing a molten zone in a Lindeman capillary[11]. In the crystal, the molecule has local *C*1-symmetry with different orientations of the ethyl groups with respect to the central trigonal-bipyramidal C_2B_3 fragment, mean B-C and B-B distances are 1.571 and 1.876 Å, respectively, the axial C. . . C distance being 2.277 Å. *Ab initio* calculations of the molecular structure indicat that rotational barriers of the ethyl groups with respect to the central frame are very small, which may be the reason of the low molecular symmetry and different orientation of the Et groups in molecule due to

Figure 38: Three-dimensional distribution of the electrostatic potential based on experimental data. The isopotential surfaces shown are blue: 0.50, red –0.03 and net 0.00 eÅ^{-1}.

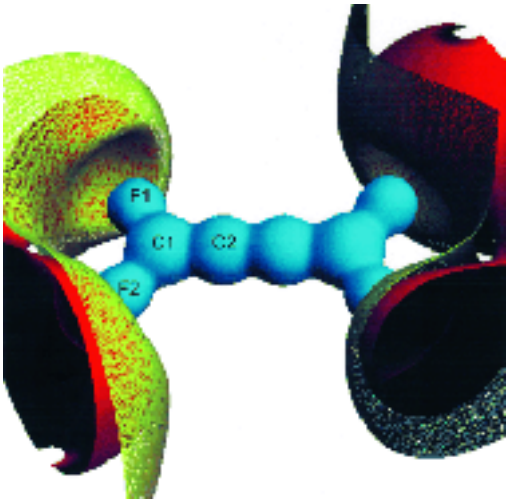

Figure 39: Chemical diagrams highlighting the molecular sketch of the studied fluorobenzenes.

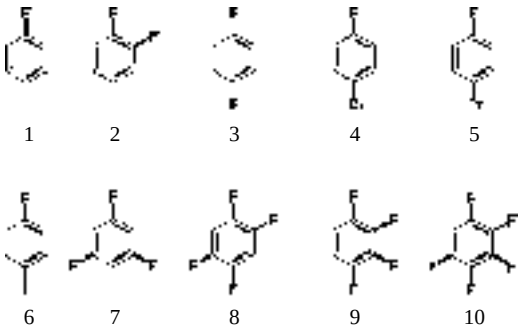

the crystal packing effects. Deformation electron density (DED) maps obtained via a conventional "X-X" method, and using a multipole refinement procedure, showed charge accumulation in the B-C bonds of the central frame (Figure 19), and these bonds were found to be essentially bent outward of the C_2B_3 cage. On the contrary, no charge accumulation was detected in the B-B bonds, thus indicating the absence of the direct B-B interactions. Positive and delocalized DED was also found in all B-C-B triangle faces of the central cage, which indicates the contribution of the multi-center bonding in the electronic structure of this formally electron-precise molecule. Topological analysis of the experimental charge density distribution has been performed

Figure 40: Possible synthons utilizing C–H. . . F interactions.

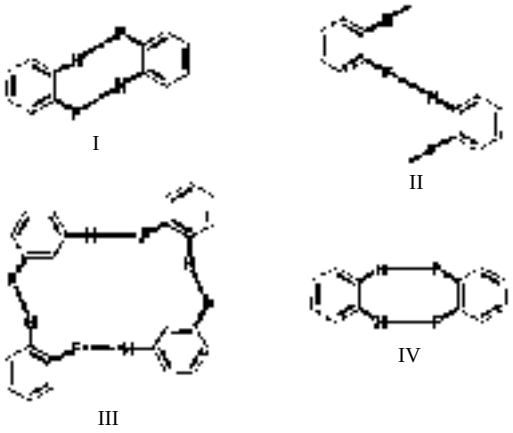

including an analysis of the Laplacian maps (Figure 20), and these data confirmed all-important features of the DED maps.

3.9. *Molecular and crystal structure of acetyl acetone*

β-diketonates are a well known class of tautomeric compounds which find immense use in organic and inorganic chemistry. The existence of keto-enol equilibrium and an understanding of the nature of the strong intra-molecular O–H. . . O hydrogen bond has been a subject of extensive studies involving the use of a variety of methods like IR, Raman, microwave and NMR spectroscopy, X-ray and neutron diffraction and quantum mechanical calculations. The molecular and crystal structure of acetylacetone (AA) was studied at 210 and 110 K in order to reveal the nature of the hydrogen bond and possible crystal disorder (Figure 21)[12]. The single crystal was grown by *in situ* crystallization from the melt using an IR laser beam producing a molten zone in a Lindeman capillary. At both temperatures the crystals are orthorhombic (space group *Pnma*, $Z = 4$) with molecules possessing a crystallographic mirror plane perpendicular to the mean molecular plane. The intra-molecular hydrogen bond is characterized by O. . . O distances of 2.541(2) and 2.547(1) Å at 210 and 110 K respectively, with the central hydrogen atom equally distributed over the two positions near the oxygens. Hence AA has two distinct potential minima that are in agreement with previous NMR data and recent quantum-chemical calculations. The bond lengths C–O and C–C in the *cis*-enol fragment have averaged values [1.291(1) and 1.402(1) Å at

Figure 41: Structural similarity between 1 and PyHF, PyNO, PhCN. (a) C–H...F mediated helices in 1. (b–d) C–H...F^-, C–H...O and C–H...N mediated helices in PyHF, PyNO, PhCN. Notice the similarity in all the structures

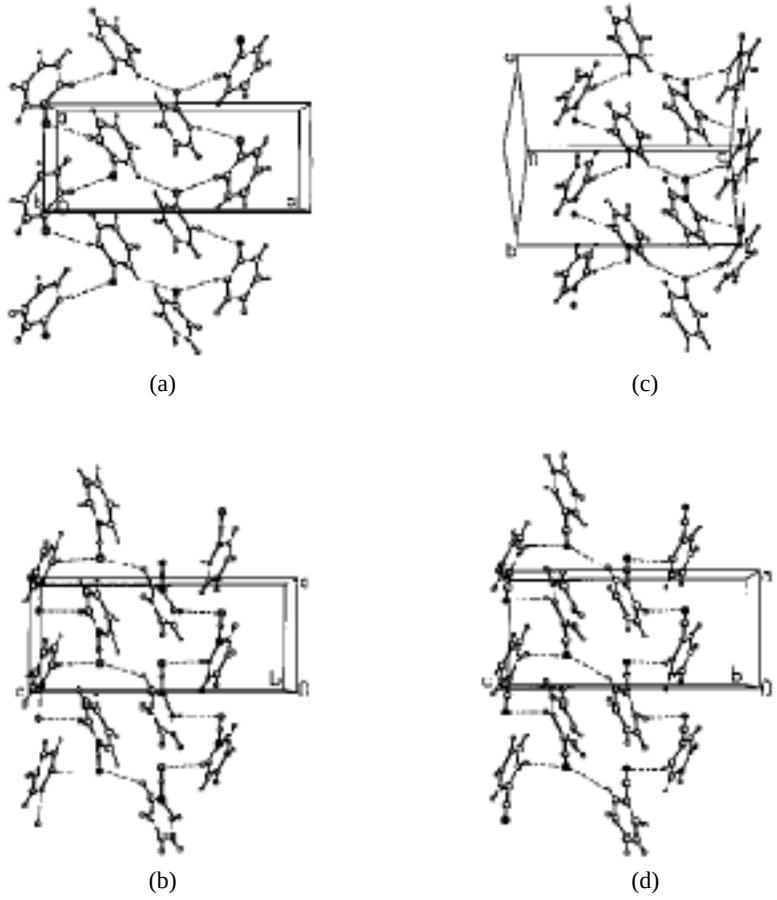

Figure 42: Structural Similarity between 3 and benzoquinone.

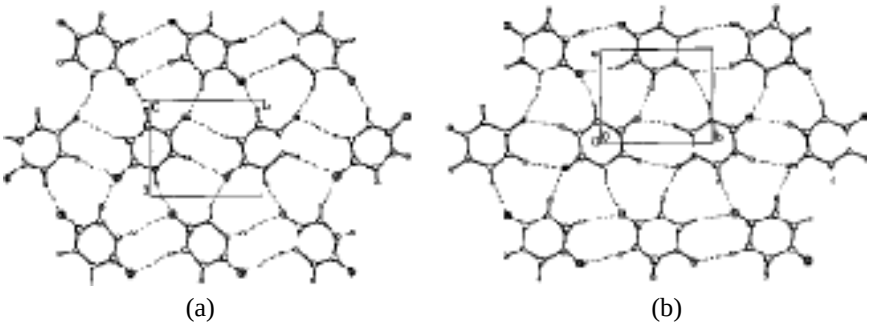

110 K] corresponding to the superposition of two enol isomers due to crystallographic symmetry. Charge density analysis in AA has been performed using the high order X-ray diffraction data at 110 K and fitted to a multipole model (Figure 22). A multi-temperature analysis of the atomic anisotropic displacement parameters cannot reveal the nature of the crystal disorder.

Figure 43: Structural Similarity between 7 and 1,3,5-triazine.

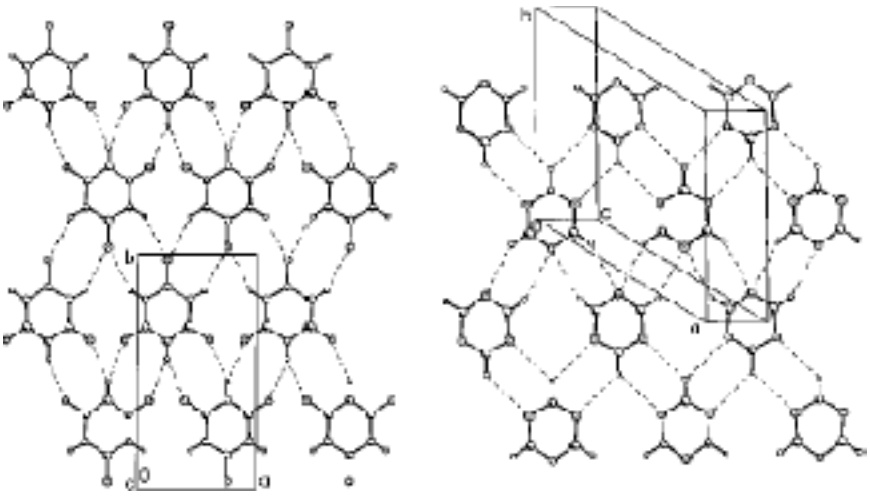

(a) (b)

Figure 44: Structural Similarity between 8 and 1,2,4,5-triazine.

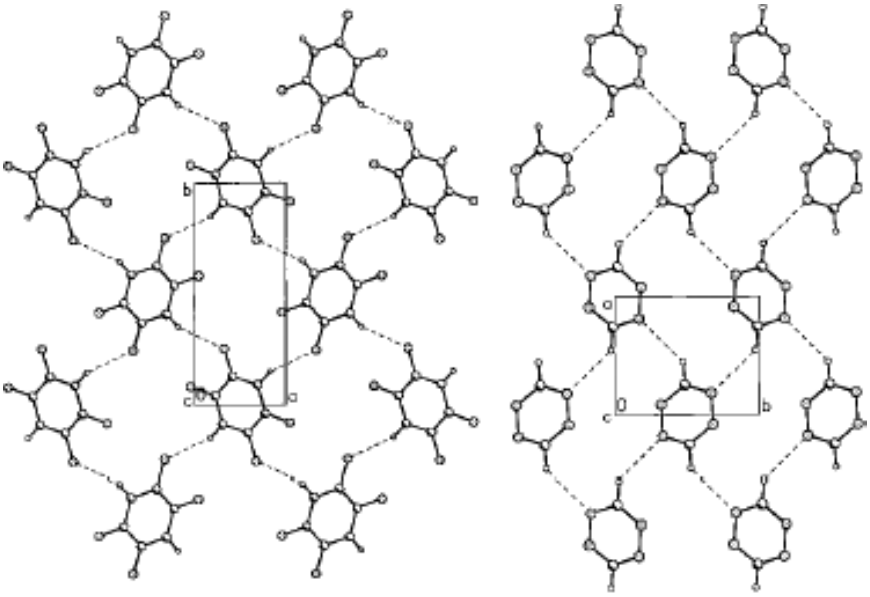

(a) (b)

3.10. *Crystal structure determination in low-melting ionic liquids*

Salts with low melting points may offer industry a cleaner, greener alternative to conventional organic solvents if problems associated with recovery and re-use can be overcome— for instance, the purification of recovered ionic liquids. If a material can form crystals on solidification, this is a good indicator that it can be purified. This year, Liverpool University chemists developed new techniques for producing crystals of ionic liquids, enabling the structures of another five to be determined for the first time—creating new world records. Studies of low-melting organic salts ('ionic liquids') are driven by intrinsic interest as well as by possible technical applications. The latter give rise to a series of practical challenges, particularly relating to purity, purification, recovery, and recycle. Zone melting, the basis of the current

Figure 45: DSC traces of 4-fluoroaniline (4FA)

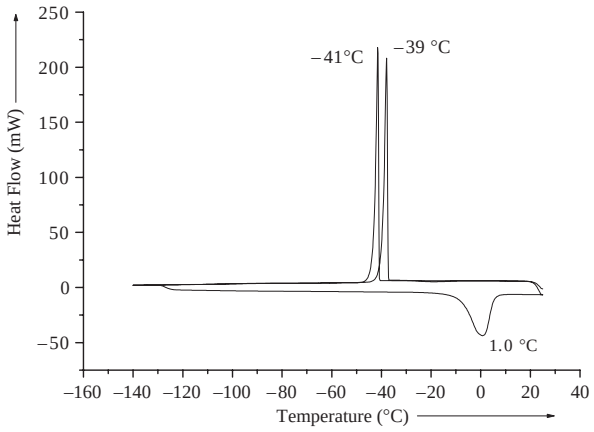

Figure 46: In-situ cryocrystallized samples of (a) 4FA (b) 2FA.

(a) (b)

Figure 47: Rotation images on the cryocrystallized sample collected before data collection (a) 4FA (b) 2FA.

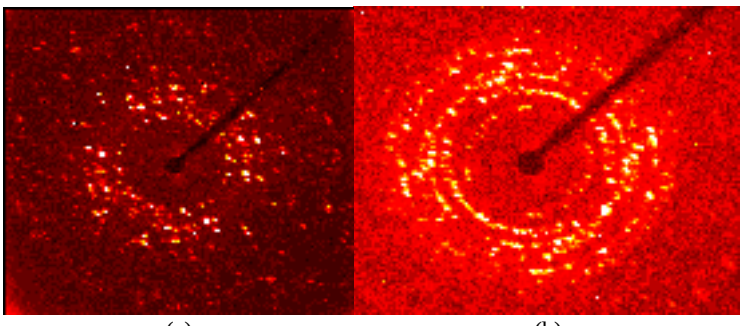

(a) (b)

study, is a possibly generic approach to ionic liquid purification and focuses attention on their phase behavior and crystallizability.

The group of A. Witherton is actively involved in the determination of the crystal structures of such low melting ionic liquids[13]. Single crystals of seven very low-melting ionic liquids, [emim]BF_4 (M.P: –1.3°C), [bmim]PF_6 (+ 1.9°C), [bmim]OTf (+ 6.7°C), [hexpy]NTf_2 (−3.6°C), and [bmpyr]NTf_2 (−10.8°C), [emim]OTf, and [emim]NTf_2, both melting at 225.7°C have been grown using a combined calorimetric and zone-melting approach

Figure 48: ORTEP view of 4FA (drawn with 50% ellipsoidal probability.)

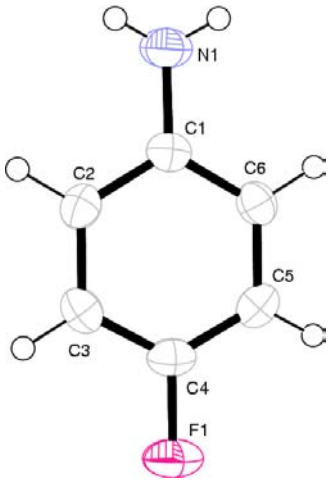

and their crystal structures determined by X-ray diffraction (Figures 23(a)–(g)).

Polymorphism in diphenyl ether

Polymorphism in diethyl ether has been identified during *in situ* crystallization via single-crystal X-ray diffraction (Figure 24)[14]. Only weak inter- and intra-molecular C–H$\cdots\pi$ interactions control the packing of the molecules in both crystal forms monoclinic centrosymmetric ($P2_1/n$) in Form I, orthorhombic noncentrosymmetric ($P2_12_12_1$) in Form II.

The ORTEPs of the two forms (hereafter I for the centric $P2_1/n$ and II for the noncentric $P2_12_12_1$) are shown in Figure 25 with atom labeling. The molecular conformations in the two forms are similar with the angles between the least-squares planes [PL1 = C1$\cdots$C6, PL2 = C7$\cdots$C12] through the phenyl rings being 88.39(7) ° and 87.60(4) ° and the ∠ C1–O1–C7 being 117.9(1) ° and 118.3(1) ° for I and II, respectively. A significant intra-molecular C–H$\cdots\pi$ interaction is the main reason for locking up the molecular conformation in each case. It is remarkable to note that angles between PL1 and PL2 deviate markedly from a theoretically (RMP2) optimized geometry using a 6-31G-basis set in Gaussian 98 [∠PL1$\cdots$ PL2 = 67.65 °.

Intermolecular C–H$\cdots\pi$ interactions control the packing of the molecules in the unit cell, thus mediating the generation of two polymorphic forms. In I, the intermolecular C–H$\cdots\pi$ interactions form a three-dimensional network of molecules (Figure 26) with C–H$\cdots\pi$ interactions involving H3 and H6 forming chains along '*a*' axis. An additional C–H$\cdots\pi$ interaction through H11 interlinks these chains. In form II, the C–H$\cdots\pi$ interactions involving H3 and H10 form a tetramer, while another C-H$\cdots\pi$ interaction via H4 links neighboring tetramers (Figure 26). Further, a weak intermolecular C–H$\cdots$O hydrogen bond links neighboring tetramers in form II. This additional C–H$\cdots$O interaction provides thermodynamic stability

Figure 49: Packing diagram of 4FA in the crystalline lattice. Dotted lines indicate C–H. . . F and C–H. . . N hydrogen bonds.

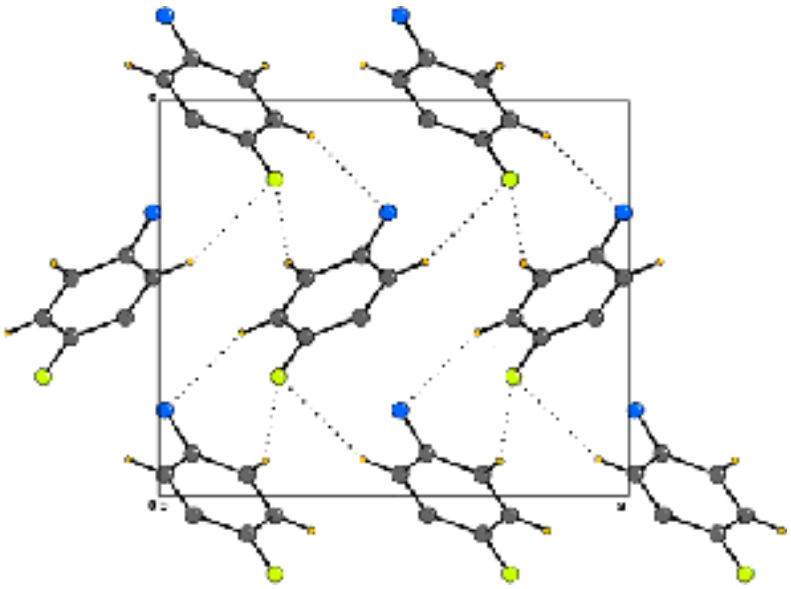

Figure 50: ORTEP view of 2FA (drawn with 50% ellipsoidal probability.)

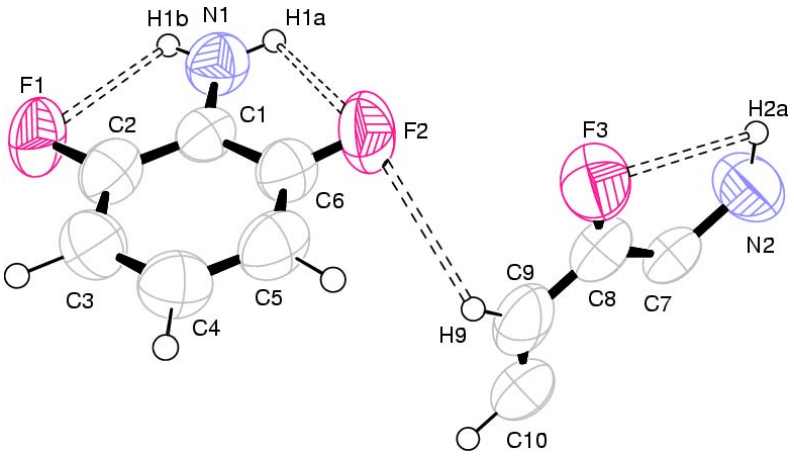

Figure 51: Packing diagram of 2FA in the crystalline lattice. Dotted lines indicate C–H. . . F and N–H. . . N hydrogen bonds alongwith N–H. . . π and π. . . π interactions.

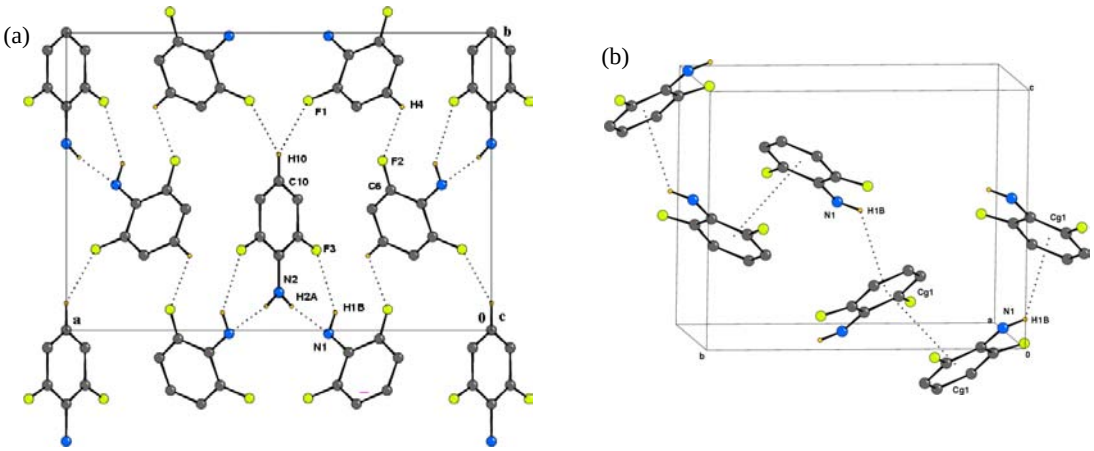

to form II and is probably responsible for the monoclinic form being a "*disappearing polymorph*" as several attempts under identical conditions resulted in access to only the orthorhombic form!

To summarize, we have demonstrated polymorphism via *in situ* crystallization for the first time in a liquid. In the current study, we have shown that, although the molecular conformations are similar, the difference in packing has resulted in the observed ideal "*packing polymorphism*".

3.11. *Gas hydrate single-crystal structure analysis*

The discovery of gas hydrates in 1811 by Sir H. Davy, were regarded as a laboratory curiosity until the mid 1930s. After clathrate hydrates of natural gases were identified as the reason for plugging of gas pipelines, extensive efforts aimed at ways to reduce the substantial costs of keeping pipelines free of gas hydrates were initiated. Interest in gas hydrates further increased when deep sea exploration identified huge reservoirs of methane gas in hydrate form, probably exceeding other fossil fuel reserves by a factor of 2.1. Structural details appeared in 1951 when Claussen proposed a structure based on *ab initio* calculations that were proven to be correct by von Stackelberg. Three main structural types of gas hydrates, named SI, SII, and SH, have been characterized in their single crystals using neutron or X-ray diffraction techniques.

Within the family of inclusion compounds, gas hydrates represent an extraordinary category. The host network consists of cages, which are built form

Figure 52: Images of *in situ* crystal growth from liquids in structures 1–4.

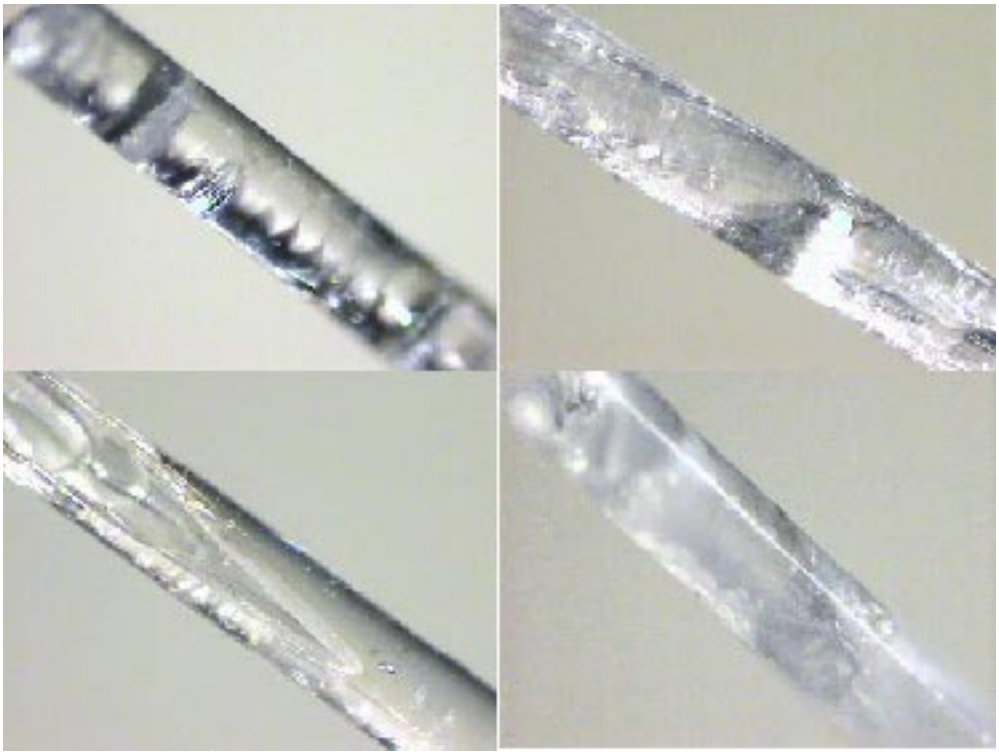

Figure 53: ORTEP plot of 1 drawn at 50% ellipsoidal probability (asymmetric unit). Dotted lines indicate intra-molecular C–H. . . F contacts. The labels indicate the atom-numbering scheme.

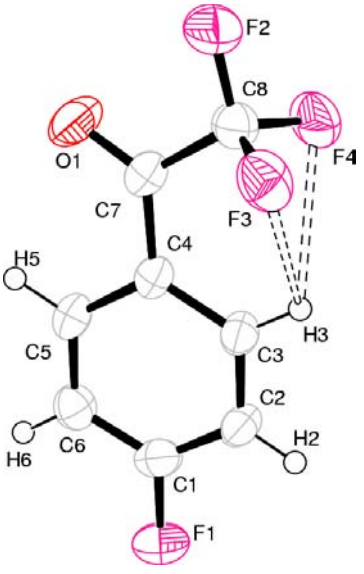

Figure 54: ORTEP plot of 2 drawn at 50% ellipsoidal probability (asymmetric unit). Dotted lines indicate intra-molecular C–H. . . F contacts.

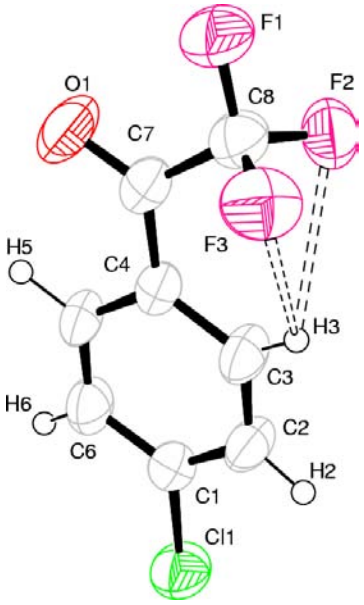

Figure 55: ORTEP plot of 3 drawn at 50% ellipsoidal probability (asymmetric unit). Dotted lines indicate intra-molecular C–H. . . F contacts.

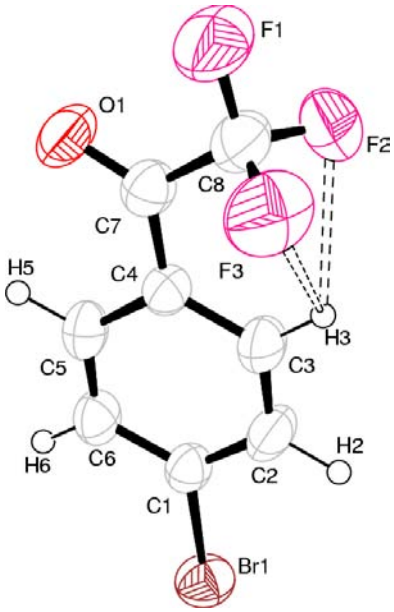

Figure 56: ORTEP plot of 4 drawn at 50% ellipsoidal probability (asymmetric unit). Dotted lines indicate intra-molecular C–H. . . F contacts.

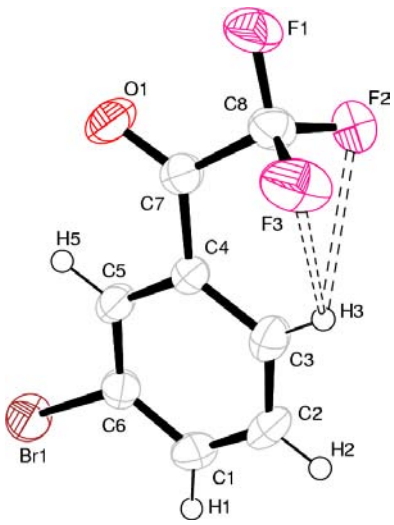

Figure 57: ORTEP plot of 5 drawn at 50% ellipsoidal probability. Dotted lines indicate intra-molecular C–H. . . F contacts. Prime denotes fluorine atom generated across the mirror plane.

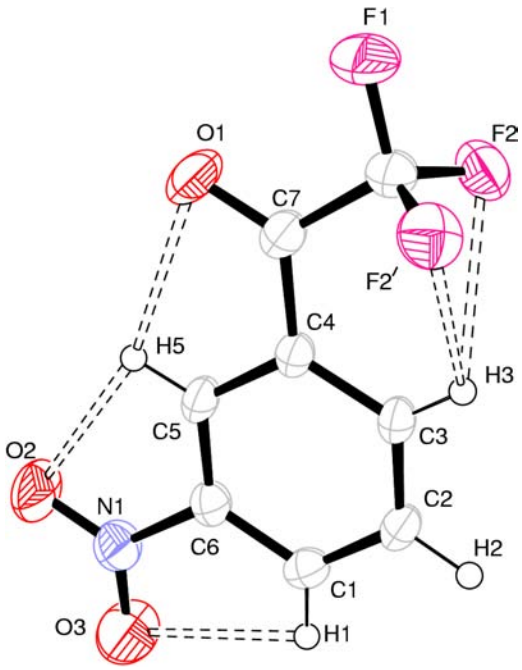

water molecules that incorporate guest molecules. The most important networks are structure I, 6X, 2Y, $46H_2O$, structure II, 8X, 16Y, $136H_2O$, and the hexagonal structure H, 1X, 3Y, 2Z, $34H_2O$, where X, Y, and Z indicate different types of cages in the clathrate hydrates, according to their size. The cages are filled with guest molecules that stabilize the host network[15]. An overview of the prominent cages and the nomenclature are presented in Figures 27–30.

The first single-crystal diffraction studies on methane, propane, methane/propane, and adamantane gas hydrates SI, SII, and SH has been performed. To circumvent the problem of very slow crystal growth, a novel technique of *in situ* co-crystallization of gases and liquids resulting in oligocrystalline material in a capillary has been developed. With special data treatment, termed oligo diffractometry, structural data of the gas hydrates of methane, acetylene, propane, a propane/ethanol/methane-mixture and an adamantane/methane-mixture were obtained. Cell parameters are in accord with reported values. On solving the crystal structures by careful modeling of the electron density, site occupation factors and thermal parameters (all are highly correlated), it was observed that methane packs in a dodecahedral cage and tetrakaidecahedral cage, acetylene in docadecahedral cage and tetrakaidecahedral cage, propane in hexakaidecahedral cage, and adamantane in icosahedral cage. Host network and guest are subject to extensive disorder, reducing the reliability of structural information. It was found that most

Figure 58: (a): Packing of 1 in the crystal lattice. Intermolecular C–H...O, C–F...F–C, $\pi...\pi$ and C=O...C=O interactions shown as dotted lines. (b): Network of C–H...F interactions in 1.

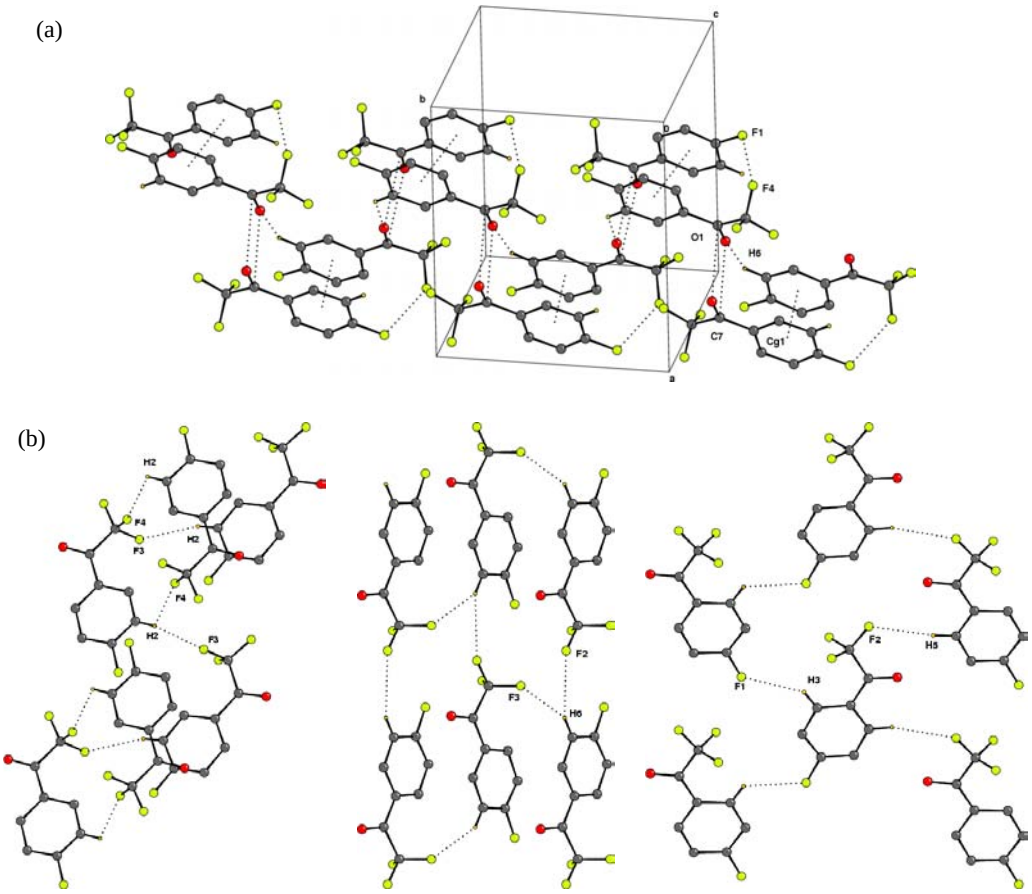

Figure 59: Packing features of 2 involving C–H...F, C–H...O and $\pi...\pi$ interactions.

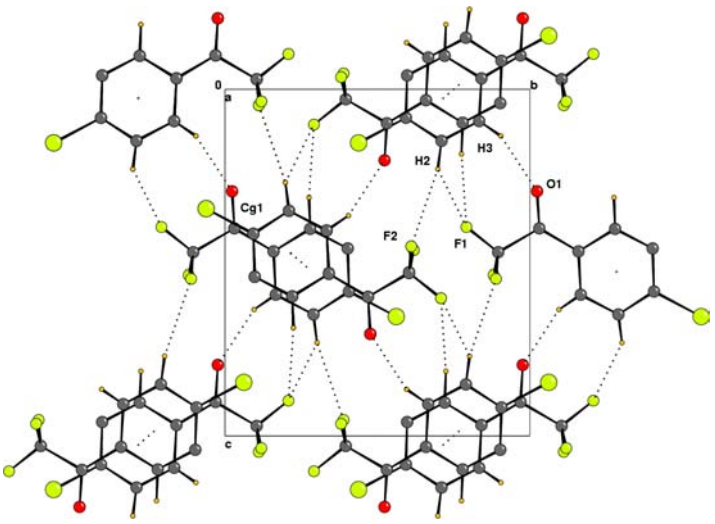

Figure 60: Regions of intermolecular interactions depicting Br...O, Br...F, C–H...F, C–F...F–C and $\pi...\pi$ interactions in 3.

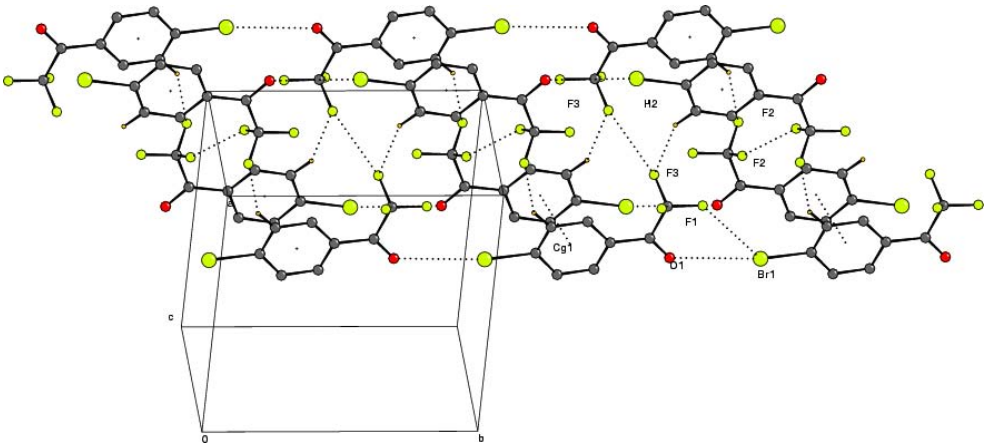

cages are fully occupied by a guest molecule with the exception of the dodecahedral cage in the acetylene hydrate, which is only filled to 60%. For adamantane in the icosahedral cage a disordered model is proposed. The packing forces, which stablize, the guest molecules in the cage (host) lattice consist mainly of hydrogen bonds and van der Waals interactions. Cryo-crystallization of multiple components results in formation of an oligocrystal and X-ray diffraction measurements on such systems is called oligodiffractometry. The physical factor, which determines which host will enter the guest lattice, is the "size" and not influenced by the chemical nature of the host.

3.12. *Co-crystallization of acetylene with acetone and DMSO*

Acetylene is widely used in welding and as a fuel for generating hot flames, is found to dissolve readily in acetone or in DMSO. Both solvents are used along with porous material to prevent polymerization when the gas is stored at elevated pressure. The acidic character of the hydrogen atoms in acetylene molecule participates in hydrogen bond formation with the oxygen atoms of the guest molecules.

In the α phase **1** the ratio of acetylene to acetone is 1:2[16], the structure indicates a three-component molecular complex with a dumbbell shape and two almost linear C–H...O hydrogen bonds. In the crystal these complexes are arranged in a herringbone fashion (Figure 31). In the β phase **2** the ratio of acetylene to acetone is 1:1. The molecules are arranged in a zigzag chain with two hydrogen bonds to the oxygen atom of each acetone molecule. One of these hydrogen bonds is nearly linear to the carbonyl group while the other is side-on (Figure 32). In addition to the relatively strong C–H...O hydrogen bonds of acetylene, several much weaker C–H...O hydrogen bonds with the methyl groups can be identified. They resemble the hydrogen bonds involving the methyl groups found in the crystal structure of pure acetone, in which stacked molecules with opposing dipoles and dimers with two C–H...O hydrogen bonds occur.

Figure 61: Regions of intermolecular interactions highlighting Br...O dimers, C–H...O, C–H...F and C–F...F–C interactions in 4.

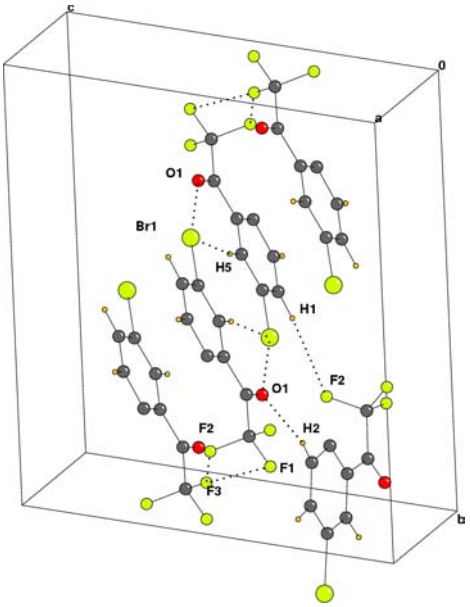

Figure 62: (a) Packing of molecules showing C–H. . . O interactions in 5. (b) Regions of intermolecular interactions showing C–H...F, C–F. . . O, C–F. . . F–C and $\pi \ldots \pi$ interactions in 5.

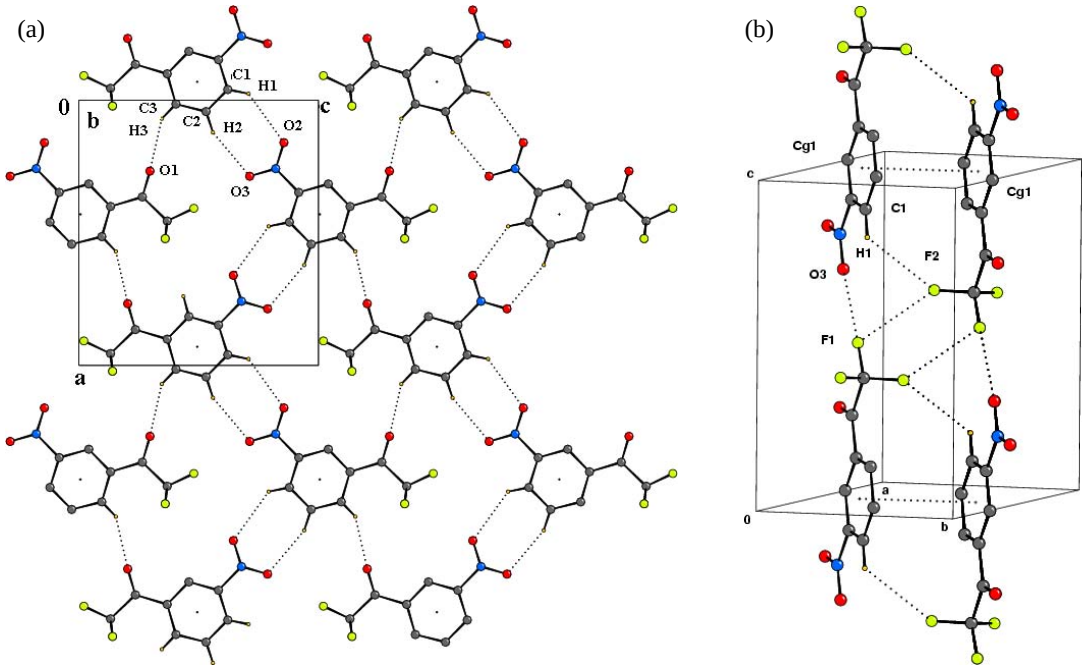

The methyl hydrogen bonds are responsible for creating the three-dimensional network with the 1:2 (zero-dimensional) complexes and the 1:1 (one-dimensional) zigzag-chains. From the viewpoint of crystal engineering and co-crystallization there is a fundamental conclusion; the packing motifs of the neat component can also be maintained in co-crystals, even when rather strong interactions are present. In the molecular complex of acetylene with DMSO, **3**, the ratio of acetylene to DMSO is 2:1. A two-dimensional network can be identified, again with one nearly linear and two additional side-on C–H. . . O hydrogen bonds (Figure 33). The pseudohexagonal two-dimensional network of triple acetylene-bridged oxygen atoms is open so that neighboring layers can interlock and still leave cavities for a third molecule of acetylene that does not participate in hydrogen bonding.

3.13. *Surprise crystal packing in an interhalogen compound—ClF*

Numerous structural investigations on interhalogen compounds have been a subject of studies related to understanding of chemical bonds. In most cases, such studies are of great importance because they provide access to important information about the electronic nature of intermolecular interactions between halogen atoms. In general, X-ray diffraction studies of neutral interhalogen compounds are rather rare, because most of them are reactive having high oxidative activity, low-melting, and boiling points, moisture sensitive and extremely difficult to handle. It was expected that the packing in ClF[17] would be similar to that observed in β-ICl, β-IBr that is zigzag or herringbone patterns, governed by orientation of dipoles with chlorine atoms surrounded by one or more fluorine atoms. Surprisingly the X-ray data show that in the crystal the individual ClF molecules form infinite planar ribbons along the screw axis which are characterized by very short Cl. . . .Cl contacts between neighbouring molecules. In each ribbon, the chlorine atoms are arranged in zig-zag fashion so each atom participates in two (symmetry equivalent) Cl. . . Cl contacts. Once contact is directed along the propagation of the F–Cl bond and the other one is perpendicular to the same F–Cl bond (Figure 34). This is the shortest Cl. . . Cl intermolecular contact in molecular crystals amongst the one known in literature. An interesting feature of the ClF crystal structure is its rather close similarity to that of chlorine, where each chlorine atom is involved in short intermolecular Cl. . . Cl contacts. In both structures there are Cl. . . Cl. . . Cl contacts but in ClF, fluorine atoms, forming ribbons, separate these

Figure 63: (a): Crystal structure of 3-fluorophenol at 150 K viewed down the '*a*' axis forming chain motifs. (b) Close C–H...F contacts observed in the crystal lattice. (c) Crystal Structure of 3-chlorophenol at 150 K. Distorted four-fold helices formed by O–H...O hydrogen bonds between two molecules in the asymmetric unit. (d) Diagram showing the actual position of the molecules along the axis of the helix is irregular.

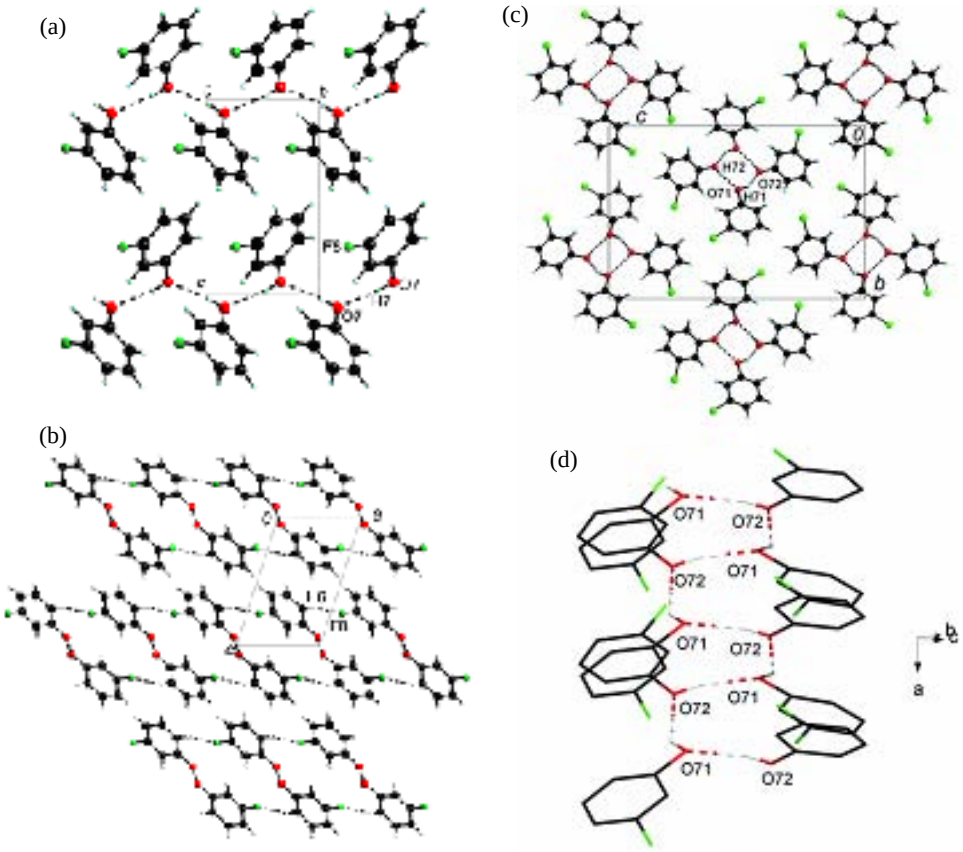

chains whereas in chlorine the neighboring chains belong to one layer. According to experimental and theoretical studies, the noble gas atoms in argon complexes of ClF were likewise found perpendicular to the F–Cl axis. From MO point of view, this interaction involves bonding between a lone pair orbital of each chlorine atom and an anti-bonding orbital of the F–Cl bond of neighbouring molecule. From the Laplacian map of the electron density in the crystal of ClF it is clear, that in the vicinity of the chlorine atoms the negative values of Laplacian are concentrated not only in F–Cl bonds but also in the directions perpendicular to the bond. These peaks are related to the charge concentration areas in the valence shell of the chlorine atom. Each of these charge concentration peaks is directed towards the neighbouring chlorine atom where the Laplacian map (Figure 35) indicates a corresponding charge depletion area. Thus each chlorine atom participates in two interactions namely a Lewis acid and Lewis base.

3.14. *Crystal structure analysis of 1,1,4,4-tetrafluorobutadiene and experimental determination of the charge density of 1,1,4,4-tetrafluorobutatriene*

In order to study the nature of C–H...F interactions and to probe the polar nature of the C–F bond, Luger *et al.*, has carried out structure determination of 1,1,4,4-tetrafluorobutadiene (1) and 1,1,4,4-tetrafluorobutatriene (2) by performing *in situ* cryocrystallization on the diffractometer[18]. Furthermore charge density calculations have been carried out on (2). Compound **1** crystallizes in the space group $P2_1/n$ with half a molecule in the asymmetric unit and possesses crystallographic C_i

Figure 64: (a): Crystal structure of phase I of chlorophenol at 150K viewed along the *b* axis, showing chains of molecules held by O–H. . . O hydrogen bonds. (b) View along the [100] showing C–H. . . Cl interactions. (c) Crystal structure of phase II of 4-chlorophenol at 150 K viewed along *a* axis. The molecules crystallize in the ring motif that forms around an approximate four-fold axis involving H31 and Cl82.

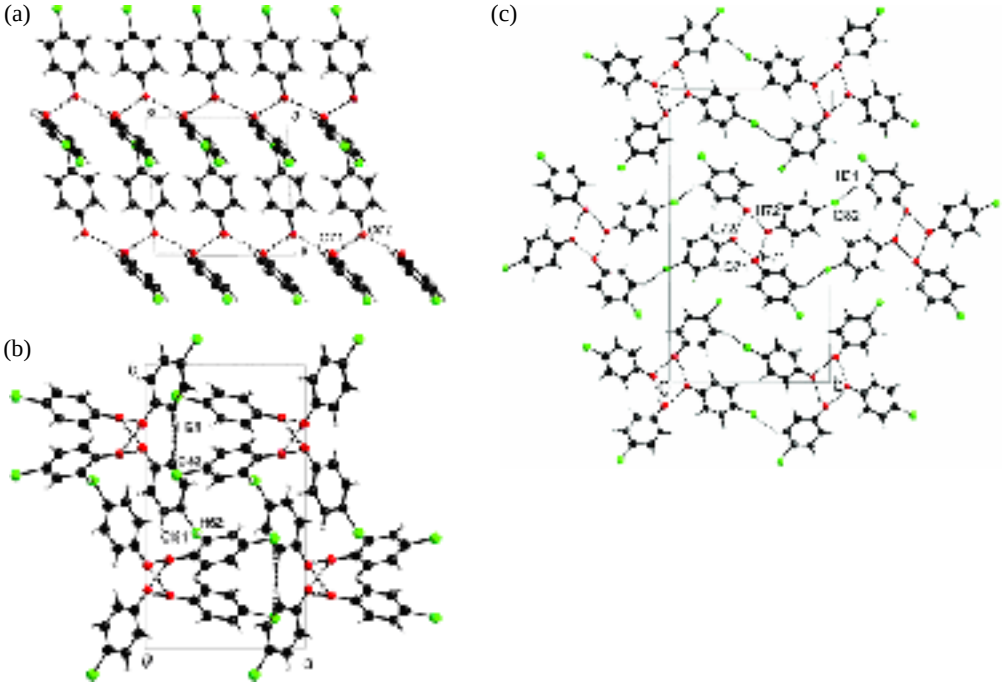

Figure 65: (a) Crystal structure of phase-I of 2-fluorophenol at 150 K. The fluorine atom is disordered across the two-fold axis running through oxygen atom O72. (b): Crystal structure of phase-II of 2-fluorophenol at 0.36 Gpa viewed along *a* axis showing chains of molecules linked by O–H. . . O hydrogen bonds. These chains are linked by C–H. . . F hydrogen bonds.

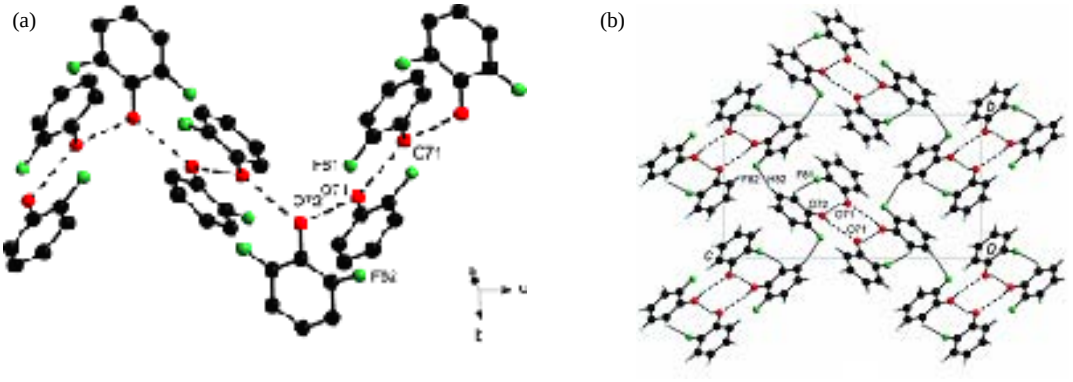

symmetry. In the solid state, the molecules have the *s-trans* conformation. The packing of the molecules is as shown in Figure 36 held by C–H. . . F contacts. A view of the *bc* plane shows the herringbone arrangement of the molecules (Figure 37).

Compound 3 crystallizes in the monoclinic space group $P2_1/c$ and the crystal packing is very similar to ethene and tetrafluoroethene. The common motif again is the herringbone arrangement.

The electrostatic potential (Figure 38) was calculated which considers a molecule to be extracted from the crystal but still contains the

Figure 66: (a) View of a single molecule of C_3F_4 in the crystal structure at 156 K, showing the atom-numbering scheme adopted. The molecule possesses crystallographically-imposed 2-fold symmetry, with the axis passing through C3 and the midpoint of C(1)–C(2) bond. Ellipsoids represent 50% ellipsoidal probability. (b) Crystal packing of C_3F_4 molecules with stacks along the crystallographic *b* axis.

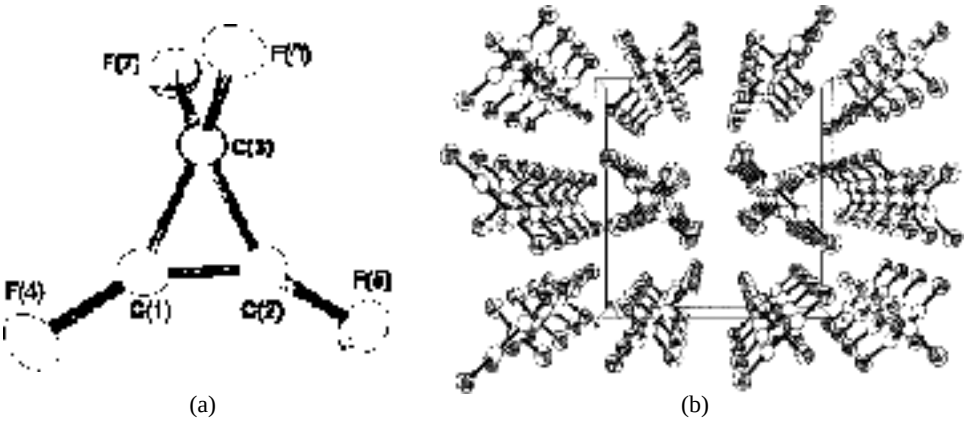

(a) (b)

Figure 67: ORTEP diagram in 2,3-Lutidine. Dotted lines indicate the diad dividing the molecule into two parts.

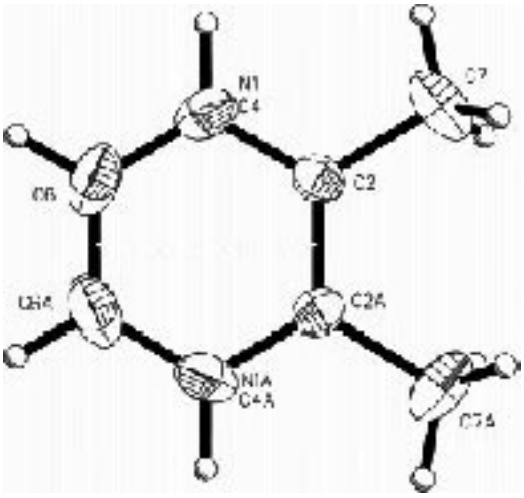

polarization effects induced by intermolecular interactions. As expected the negative potential is concentrated around the fluorine atoms and the positive potential along the molecular axis.

3.15. ***Crystal structures in fluorinated benzenes***

The existence and nature of C–H…F–C interactions in crystalline fluorobenzenes (Figure 39)[19] has been studied by Boese *et. al.*, to evaluate the weak acceptor capabilities of the C–F group. All the compounds contain C, H and F only and are liquids at room temperature. Hence crystals were grown *in situ* on the diffractometer. It was concluded that only when the carbon acidity is enhanced by electron withdrawal by fluorine atom is the hydrogen bond nature of the C–H…F interactions revealed. The behavior of organic fluorine is different compared to the other halogens. Figure 40 highlights some of the possible synthons utilizing fluorine as a design element.

Fluorobenzene, **1**, bears a close relationship to pyridinium fluoride, pyridine 1-oxide, and benzonitrile (Figure 41) at the level of individual interactions, showing that the nature and character of the structure determining intermolecular interactions in these four crystal structures are the same. It may be adduced that the C–H…F interaction albeit weak, is important in the adoption of the observed crystal structure. Similarly, 1,4-difluorobenzene, **3**, and 1,4-benzoquinone are related, (Figure 42) the C–H…F interactions in the former playing the same structural role as the C–H…O interactions in the latter. A comparison of **3** with the unsymmetrical 1,4-dihalogenated benzenes, **4**-**6** indicates the importance of C–H…F interactions in these structures. With an increase in the F content of the molecules, the C–H acidity also increases and the C–H…F interactions in 1,3,5-trifluorobenzene, **7**, and 1,2,4,5-tetrafluorobenzene, **8**, become stronger and more important. Compounds **7** and **8** are structurally very similar to 1,3,5-triazine (Figure 43) and

Figure 68: Packing diagram in 2,3-Lutidine depicting C–H...N interactions forming molecular chains.

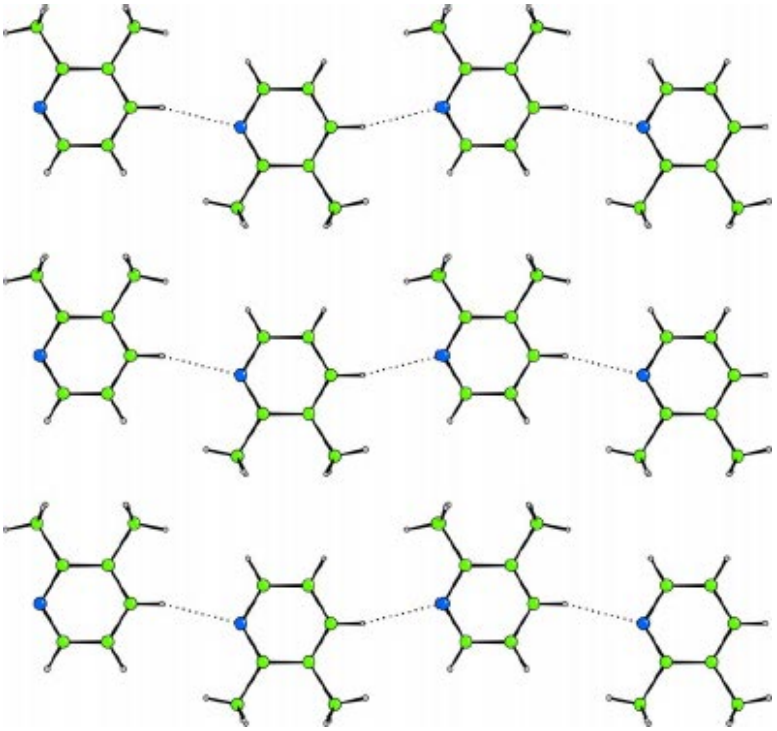

Figure 69: ORTEP diagram in 2,5-Lutidine.

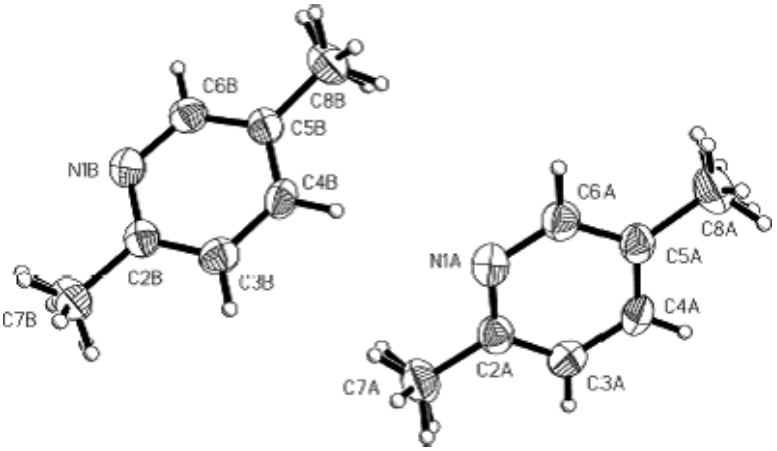

1,2,4,5-tetrazine (Figure 44), and this similarity further strengthens the argument that C–H…F interactions resemble C–H…N interactions and provides evidence for their description as weak hydrogen bonds. 1,2,3,4-Tetrafluorobenzene, **9**, is polymorphic but the role of the C–H…F interactions in the two forms is similar. It is concluded that only when the carbon acidity is enhanced to the levels of the compounds in the present study, is the hydrogen-bond nature of the C–H…F interaction even revealed. This study also demonstrates that the C–F group prefers to form C–H…F interactions rather than F…F contacts. The behavior of organic fluorine in crystal packing is therefore quite different from the heavier halogens. The C–H…F interaction has the characteristic of weak hydrogen bonds and hence can be of utility in crystal design and engineering.

Figure 70: Packing diagram in 2,5-Lutidine, depicting C–H...N interactions forming molecular chains.

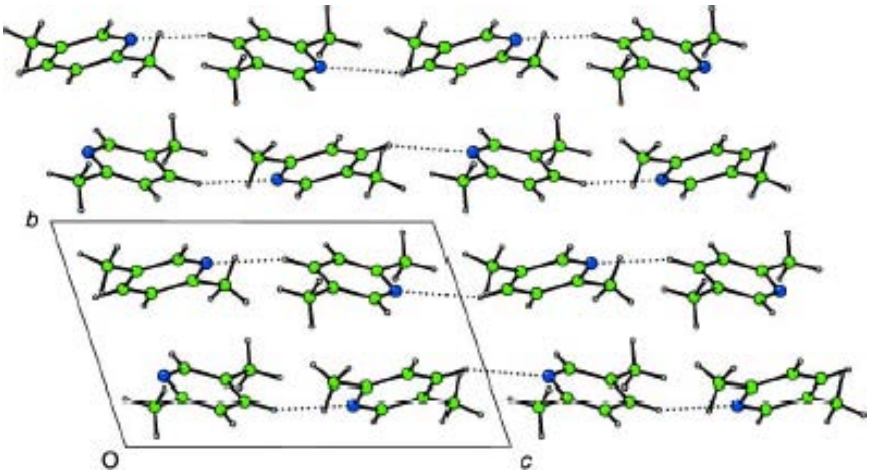

Figure 71: ORTEP diagram in 2,6-Lutidine.

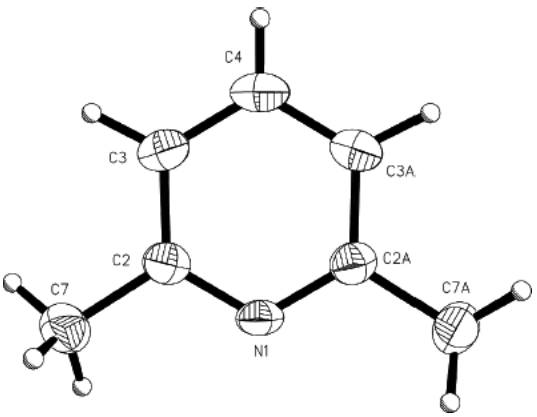

3.16. *Crystal structures in fluorinated amines*

4-Fluoroaniline (4FA) [M.P = −38 °C (from DSC) B.P = 186–188 °C] and 2-Fluoroaniline (2FA) [M.P = −73°C (from DSC), B.P = 182–183°C] are liquids[20]. A Lindemann glass capillary of ∼2.5 cm in length and 0.3 mm in diameter was filled with the fluoroamine, sealed by flame and mounted on the Bruker AXS X-ray diffractometer equipped with SMART APEX CCD area detector. Solidification by ramping at fast rates (360 K/h, 300 K/h) resulted in the formation of glassy material with one exception at a ramping rate of 100 K/h resulting in a polycrystalline solid.

Based on the features displayed by Differential Scanning Calorimetry (DSC) analysis (Figure 45), on cooling very slowly at 30 K/h using an OXFORD Nitrogen cryosystem it was observed that complete solidification of the liquid in the capillary took place at 220 K (−53 °C) and at 170 K (−103 °C) in case of 4FA and 2FA. No such features were observed for 3FA and hence repeated attempts to crystallize failed. In the first attempt, with the cooling rate of 30 K/h we could induce crystallinity in the sample and hence avoid possible glass formation. In order to obtain a single crystal inside the capillary the solid was annealed by shifting the nitrogen stream away from the capillary, the solid was allowed to melt partially inside the capillary and then resetting the nitrogen stream at a very slow rate. This procedure was repeated manually until a cylindrical single crystal was obtained (Figures 46). A rotation photograph of the solidified samples prior to data collection was taken (Figures 47). The quality of the diffraction spots obtained was very good. The indexed reflections correspond to an orthorhombic **(4FA)** and monoclinic **(2FA)** cell respectively.

Figures 48 and 50 give the ORTEP of 4FA and 2FA with the corresponding atom numbering. In 4FA, the molecules pack in the non-centrosymmetric space group $Pca2_1$ with essentially weak interactions (Figure 49). The interaction network is built based on C–H...N (involving H3) and C–H...F interactions (involving H2 and H6).

In case of 2FA, the asymmetric unit contains one and a half molecule (Z = 12 in the unit cell). The fluorine atom is disordered with occupancies of 0.73(2) and 0.27(2) for the first molecule while the second has occupancy of 0.50(2) with the crystallographic *diad* passing through the molecule. Figure 51 shows the packing in the unit cell with a strong N–H...N hydrogen bond involving the hydrogen atom H2A. It is noteworthy that only the fluorine atom is statistically disordered and further generates several intra- and intermolecular

Figure 72: Packing diagram in 2,6-Lutidine along the 1 axis.

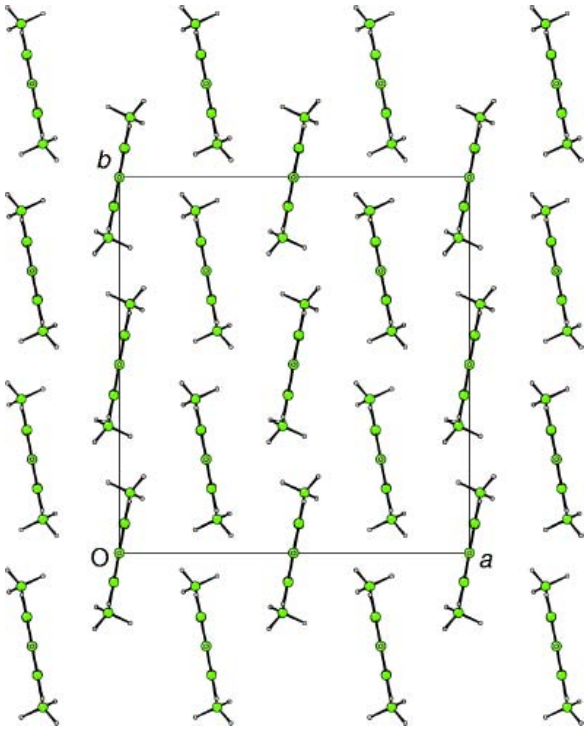

Figure 73: ORTEP diagram in 3,4-Lutidine.

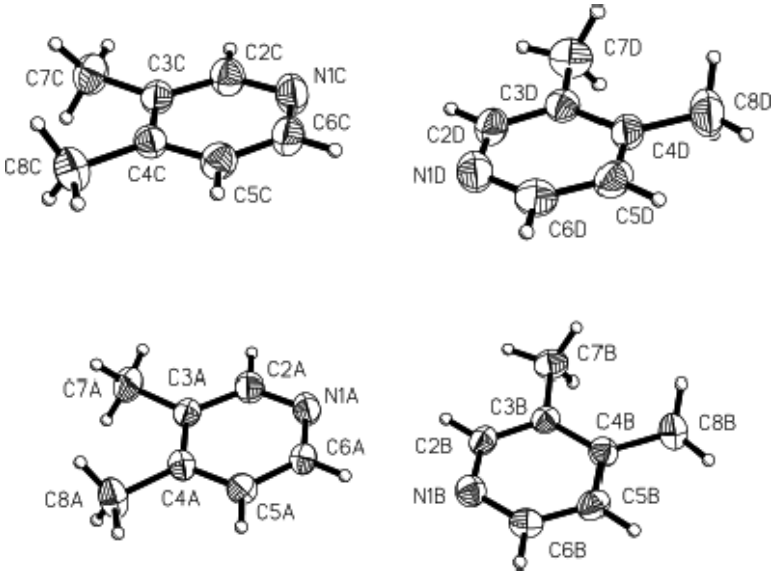

interactions of the type N–H…F (involving H1A, H1B and H2A) and C–H…F (involving H4 and H10) forming molecular chains along *b* and *c* axis. The presence of N–H…π using H1B forming molecular chains along *c* axis and π…π van-der Waals interactions with a stacking distance of 3.720(5) Å provides additional stability. It is noteworthy that the density of 1.31g/cm^3 in case of 2FA is lower than in 4FA. To summarize, the two crystal structures studied via *in situ*

Figure 74: Packing diagram in 3,4-Lutidine along the 1 axis.

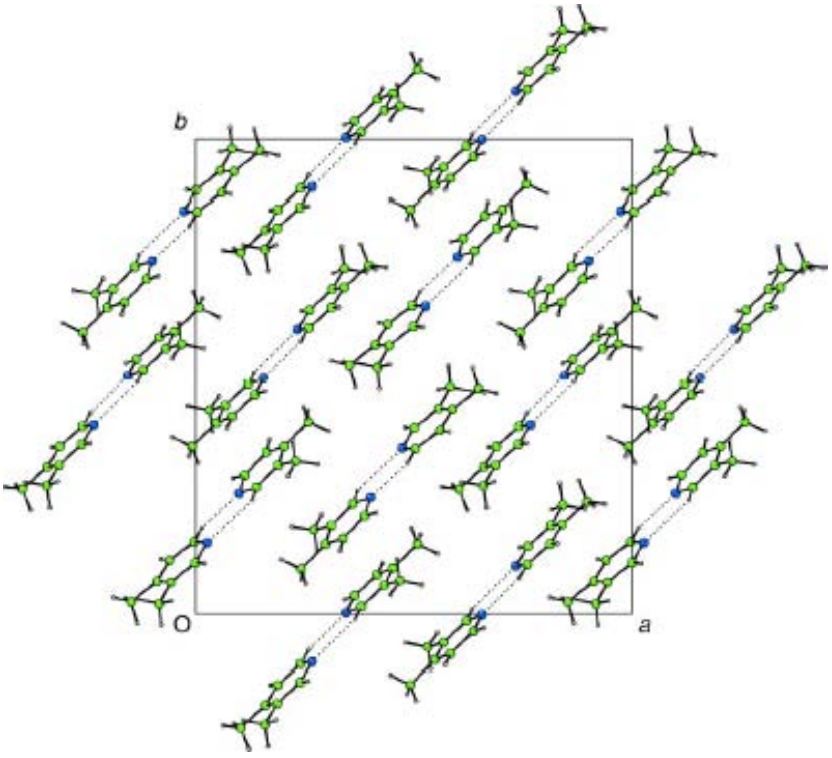

Figure 75: ORTEP diagram of (1S)-(-)-β-Pinene.

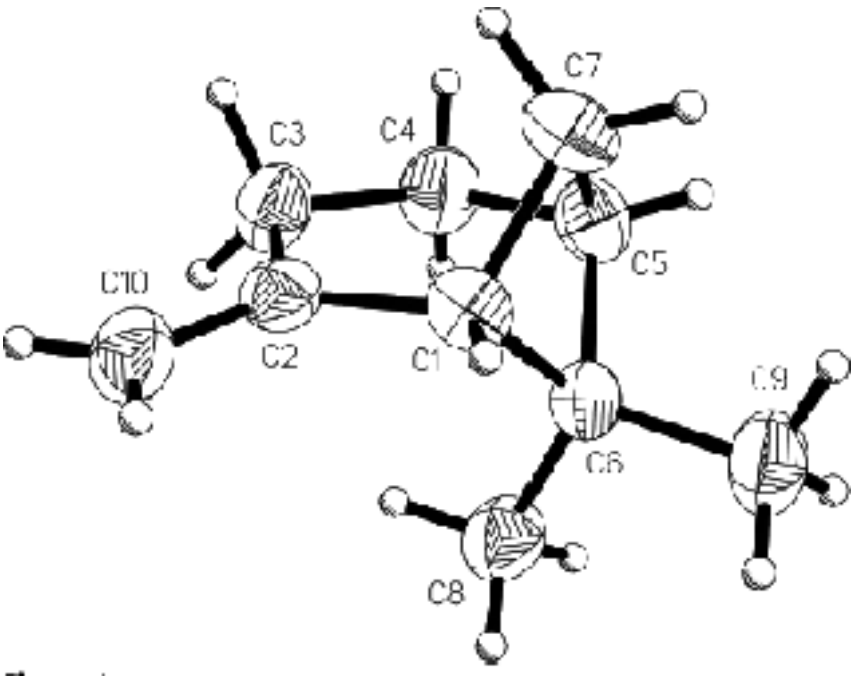

Figure 76: ORTEP diagram of (1S)-(-)-α-Pinene.

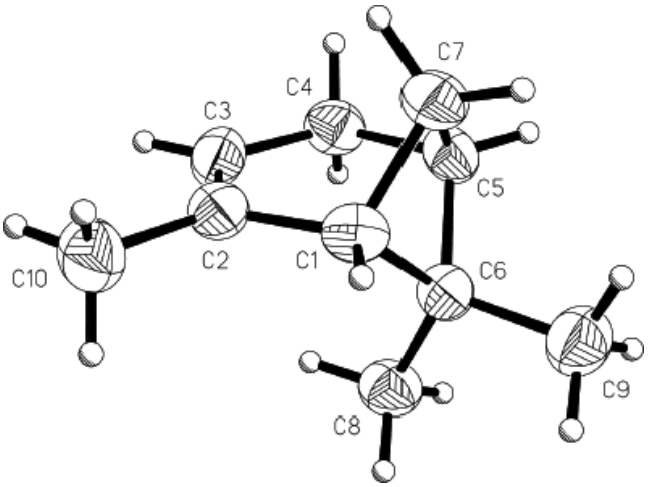

cryocrystallisation demonstrate that the presence of interactions involving fluorine in directing packing motifs can also provide additional stability acting cooperatively with strong hydrogen bonds. Further even in presence of disorder it appears that crystallization is driven through weak yet strongly directional interactions involving fluorine.

3.17. *Crystal structures in trifluorinated acetophenones*

Inter- and intra-molecular interactions involving halogens in molecular crystals have been reviewed extensively, with an emphasis to study variable hydrogen bonding features. Interactions involving chlorine and bromine in particular have been recognized and analyzed in terms of their directional preferences and in terms of the strength of their interaction. However, in recent times intermolecular short contacts involving organic fluorine have been recognized and well documented in the literature though the nature of these interactions is yet to be understood. In the light of the controversy regarding the participation of organic fluorine to involve in weak intermolecular interactions, short contacts (distance less than sum of the van der Waal radii of the participating atoms) of the type C–H…F, C–F…C_π and C–F…F–C have been evaluated. Database studies on halogen containing small molecules as well as in proteins and peptides bring out the importance of such interactions and their use as possible tools in crystal engineering. It is noteworthy that single crystal studies on *p*-Cl, *p*-Br, and *p*-I substituted acetophenones exhibit short X…O contacts only for the heavier halogens, Br and I, while Cl prefers

Figure 77: ORTEP of γ-terpinene.

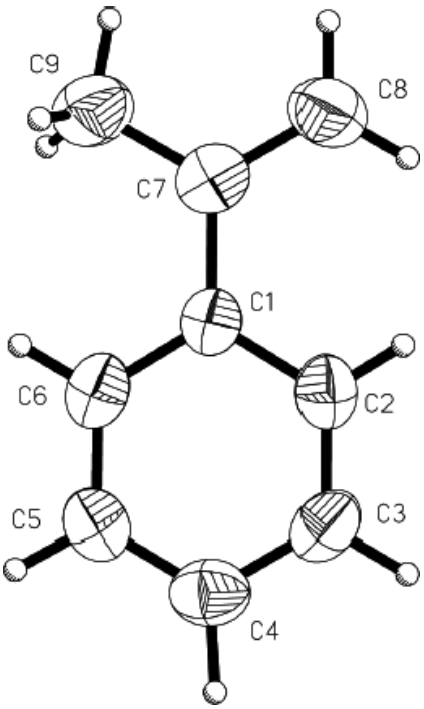

to form C–H…Cl contacts in lieu of Cl…Cl or Cl…O contacts. In this article, we explore structures of low melting trifluoroacetophenone (TFA) derivatives via *in situ* cryocrystallization techniques to analyze interactions involving fluorine, chlorine and bromine in the presence of a $-CF_3$ group. Further the molecules have been choosen

Figure 78: Packing diagram of γ-terpinene. Dotted lines indicate intermolecular C–H$\ldots\pi$ interactions.

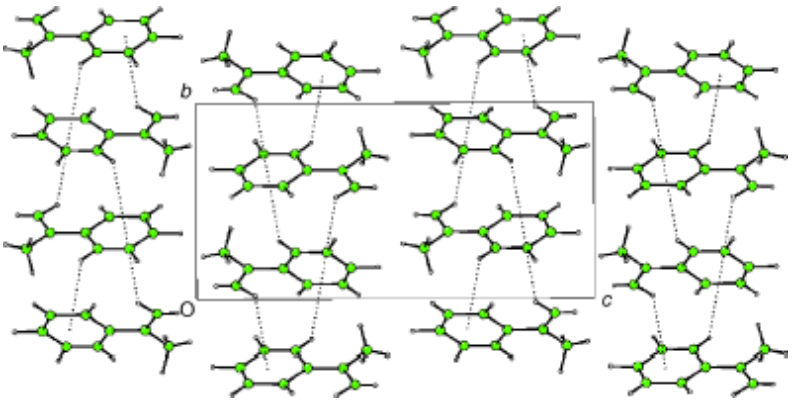

such that the $-CF_3$ moiety locks up the conformation via intra molecular C–H$\ldots$F contacts.

In combination with inputs from Differential Scanning Calorimetry (DSC), which suggest pathways for the growth of single crystals, it has become possible to evaluate intermolecular interactions as and when crystals grow. Crystal and molecular structures of five low melting solids, 1-(4 -fluorophenyl)-2,2,2-trifluoroethanone (**1**), 1-(4- chlorophenyl)-2,2,2-trifluoroethanone (**2**), 1-(4- bromophenyl)-2,2,2-trifluoroethanone (**3**), 1-(3- bromophenyl)-2,2,2-trifluoroethanone (**4**) and 1-(3- nitrophenyl)-2,2,2-trifluoroethanone (**5**) to compare the packing features with different halogens at the *para* position (**1-3**),-Br at *meta* position (**4**), a nitro group at the *meta* position (**5**) respectively, have been analyzed in this context[21] (Figure 52). ORTEP diagrams depicting the molecular structures of all the cryocrystallized samples are given in Figures 53–57.

Compound 1 belongs to the centrosymmetric monoclinic space group $P2_1/c$ and the packing in the lattice is through a network of C–H$\ldots$O, C–H$\ldots$F, and C–F$\ldots$F–C along with aromatic $\pi\ldots\pi$ interactions (Figure 58(a)). In addition, dipolar C=O$\ldots$C=O interactions involving the carbonyl group [$d = 3.213$Å] stabilize the crystal structure. The occurrence of an intermolecular C–F$\ldots$F–C interaction [2.987(2) Å] involving the *p*-substituted fluorine atom (F1) with one of the fluorine atoms (F4) of the $-CF_3$ group is a unique feature in this molecule. Even though the sum of the van der Waals radii of fluorine atoms limit to 2.94 Å, it is to be noted that the position of the minimum in the intermolecular potential is about 0.4 Å longer than the sum of the van der Waals radii. The atom F1 further connects to the atom H3 resulting in a C–H$\ldots$F contact. Several other C–H$\ldots$F contacts

Figure 79: ORTEP diagram in 2-picoline.

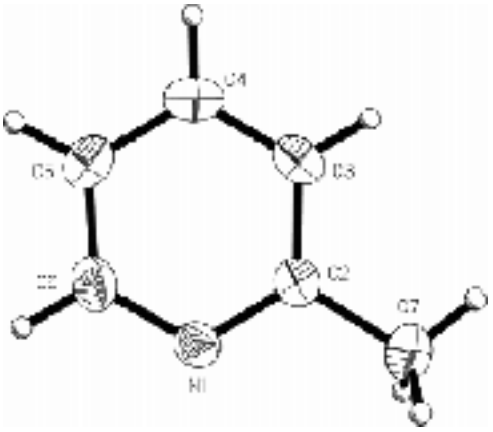

Figure 80: ORTEP diagram in 3-picoline.

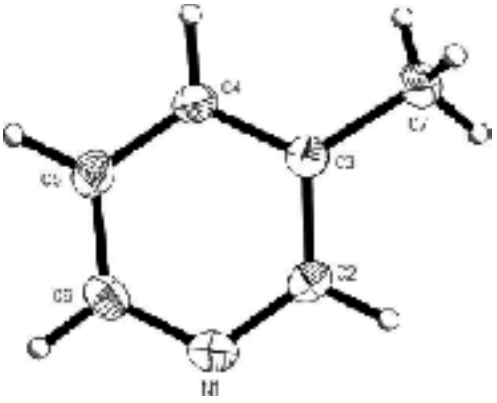

Figure 81: ORTEP diagram in (1R)-(-)-Fenchone.

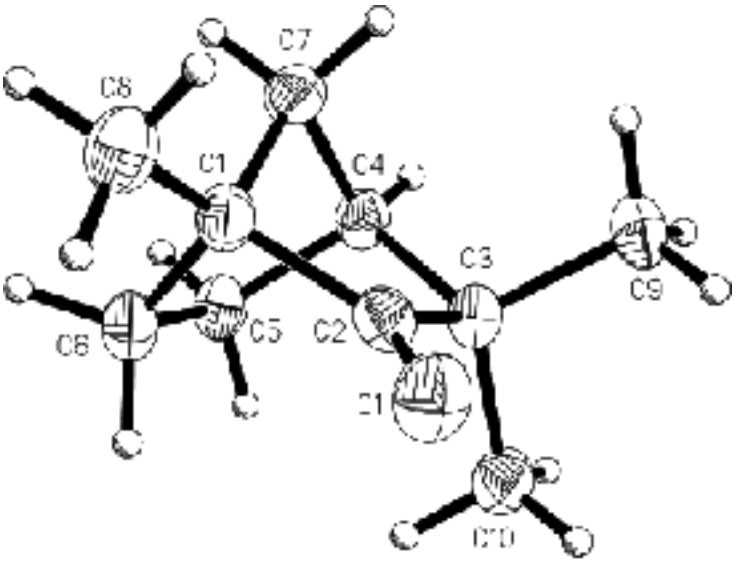

Figure 82: The "Unicorn" represents the mystical animal.

involving electronically different fluorine atoms F1 connected to C (aromatic carbon) and F2, F3, F4 of the trifluoromethyl group generate the connectivity motif in the supramolecular assembly. Atoms F2 and F3 form bifurcated intermolecular interactions involving H5, H6 with F2 and H2, H6 with F3 respectively forming molecular chains along the *b* axis, which also encompass an additional C–H…O contact (Figure 58(b)). Further, atom F4 forms dimeric units, involving hydrogen H2 providing additional stability. Subsequent stability is provided by aromatic $\pi \ldots \pi$ stacking interactions with a separation distance of 3.941(1) Å [Cg1: center of gravity of the aryl ring].

Compound 2, with chlorine atom in the *para* position, crystallizes in a non-centrosymmetric space group $P2_12_12_1$, the corresponding acetophenone derivative also having crystallized in the same space group symmetry. It was observed that C–H…Cl contacts stabilize the packing in

Figure 83: An ORTEP view of ethane-1, 2-diol, showing the atom numbering scheme. Displacement ellipsoids are drawn at 50% probability level and hydrogen atoms are shown as small spheres of arbitrary radii.

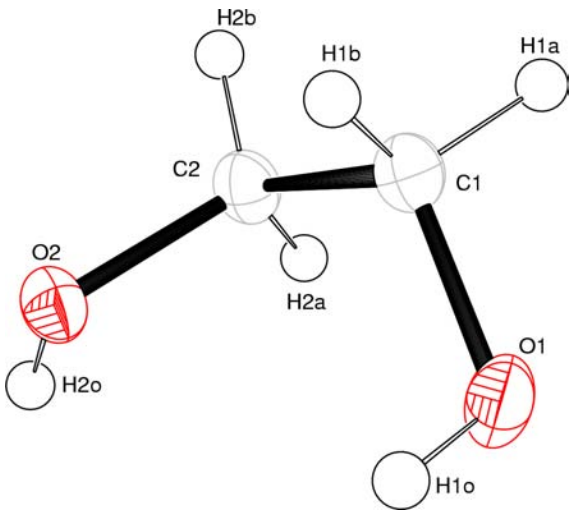

Figure 84: Packing view of the compound forming O–H...O, C–H...O hydrogen bonds generating a sheet-like structure.

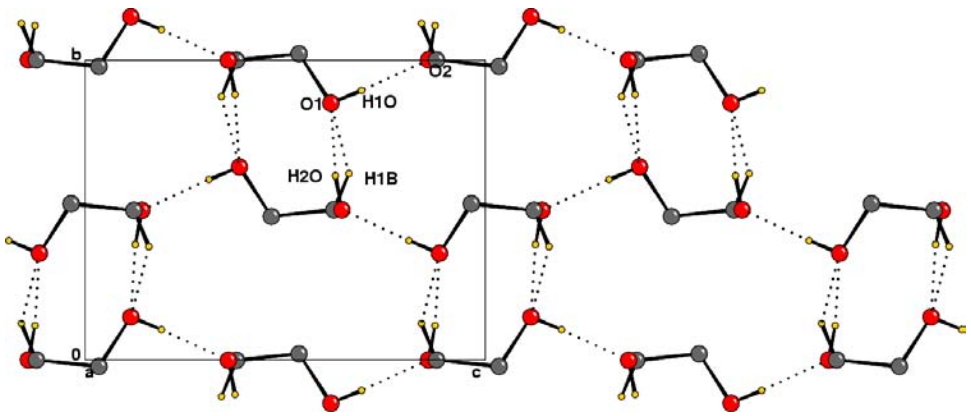

para chloro acetophenone instead of the expected Cl...O or Cl...Cl contacts due to the weak Lewis acid character of the chlorine atom. However, in Compound **2**, C–H...Cl interactions are entirely absent and C–H...F and C–H...O intermolecular contacts along with the presence of aromatic stacks along the *a* axis, the stacking distance being 3.841(3) Å [Cg1: center of gravity of the aryl ring] (Figure 59) stabilize the crystal structure. Atom F1 is involved in the formation of bifurcated interactions, involving hydrogen H2 and H5 forming molecular chains along the crystallographic *c* and *b* axis in conjunction with C–H...O interaction (involving H3), providing the overall stability. Further atom F2, involving hydrogen H2 forms molecular chains along the crystallographic *a* axis.

The *p*-bromo **compound 3**, crystallizing in the space group $P2_1/c$ exhibits a well-defined Br...O [Br1...O1 = 3.380(5) Å ∠C1-Br1...O1 = 170.4°; Figure 60], short contact, the observed result corroborates with the fact that bromine participates in formation of linear and directional halogen bond. An exceptional Br...F contact [Br1...F1 = 3.337(4) Å] forming an infinite motif along the crystallographic *b* axis provides further stability along with $\pi...\pi$ aromatic interactions with a stacking distance of 3.739(4) Å, resulting in an overall sheet-like structural motif [Figure 4(b)]. The

Figure 85: Static deformation electron density map with the oxygen lone pairs indicating absence of intra-molecular H-bond. Contours are drawn at 0.05e/Å^3 interval. Red lines indicate positive contours, blue dotted lines indicate negative contours and blue dashed lines indicate zero contour.

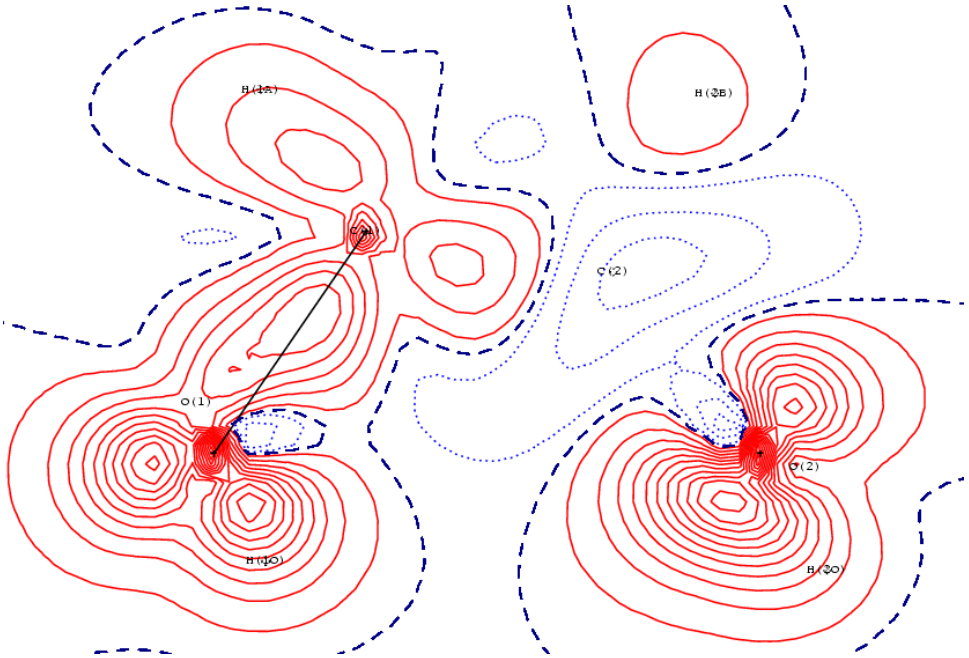

remaining two fluorine atoms of the $-CF_3$ group are involved in short F…F contacts [F2…F2=2.905(5) Å and F3…F3 = 2.941(5) Å; with C8–F2…F2 and C8–F1…F1 angle being equal to 146.8 ° and 164.8° respectively (Type I contact). There is an intermolecular C–H…F interaction, involving H2, forming chains along the crystallographic screw *b* axis. It is of interest to note that there are no C–H…Br contacts in compound **3** whereas the corresponding *para* bromo acetophenone has several additional C–H…Br contacts.

Meta-bromo substituted **compound 4** crystallizes *in situ* in the space group $P2_1/c$. Short dimeric Br…O contacts [Br1…O1 = 3.332(2) Å; ∠C6-Br1…O1 = 158.3°; Figure 61] are observed in the crystal packing. A rare C–H…Br interaction [H5…Br1 = 3.04(4) Å, ∠ C5–H5…Br1 = 171.2°] involving the hydrogen atom H5 is also seen as a consequence. A C–H…F interaction, involving H1 forming chains along screw *b* axis, along with a C-H …O hydrogen bond involving H2 forming chains along *c* glide plane generates a two-dimensional sheet like structure. Short Type II F…F contacts involving fluorine atoms C8–F3…F1–C8 and C8–F3…F2–C8 forms a triangular motif with distances 2.783(3) Å and 2.995(3) Å and angles 162.8° and 151.8° respectively. It is interesting to note that even though the molecules are arranged parallel to each other the distances prohibit aromatic stacking interactions.

Compound 5 was investigated in order to get a comparison with respect to the halogen interactions, the presence of the *meta* nitro group bringing in additional interactions. As can be seen from the ORTEP diagram three intra molecular C–H…O interactions render the entire molecule to adopt a flat conformation and the space group *Pnma* with Z = 4 ensures that except fluorine atom F2, the rest of the atoms lie on the crystallographic mirror plane (y-coordinate = 0.2500). The packing hence is controlled through intermolecular C–H…O interactions (involving hydrogen H1, H2 and oxygens O2, O3 of the nitro group) resulting in formation of molecular "sheets" along the crystallographic *a* axis related by glide plane (Figure 62(a)). An additional C–H…O interaction (involving H3 and carbonyl oxygen atom O1) generates a sheet-like structure in the *ac* plane. Remarkably, a short F…O contact [C8–F1…O3–N1 = 2.894(3) Å], a C–H…F intermolecular interaction (involving H1 and F2), a short C–F…F-C intermolecular contact [C8–F1…F2–C8 = 2.982(2) Å] and a $\pi\ldots\pi$ stacking interaction [stacking distance = 3.750(1) Å] provide interlayer stability (Figure 62(b)). It is noteworthy that the crystal structure of 3-Nitroacetophenone has both

the acetyl and nitro groups out of planarity with the dihedral angles 9.4(2)° and 1.8(2)° respectively unlike compound **5**, even though the sheet like structure in the *ac* plane is generated by similar C–H…O contacts.

3.18. *Chlorophenols and fluorophenols at low temperature and high pressure*

2-Fluorophenol, 3-Fluorophenol and 3-Chlorophenol were re-crystallized from frozen solids at 260, 263 and 283 K. All compounds were also crystallized by the application of high pressure (0.36, 0.12 and 0.10 GPa). While 3-fluorophenol and 3-chlorophenol yielded the same phases[22] under both conditions, different polymorphs were obtained for 2-fluorophenol. 4-Chlorophenol was crystallized both from the melt and from benzene to yield two different ambient-pressure polymorphs; crystallization from the melt at 0.02 GPa yielded the same phase as from benzene at ambient pressure. 3-Fluorophenol is unusual in forming a hydrogen-bonded chain along a 2_1 screw axis. Such behaviour is usually only observed for small alcohols, but here it appears to be stabilized by intermolecular C–H…F hydrogen-bond formation. 3-Chlorophenol is a more typical large alcohol and emulates a fourfold screw axis with two independent molecules positioned about a 2_1 axis, although there are significant distortions from this ideal geometry. The two phases of 4-chlorophenol consist of chains or rings connected by C–Cl…H interactions. The low-temperature and high-pressure polymorphs of 2-fluorophenol consist of chains of molecules connected through OH…OH hydrogen bonds; while inter-chain C–H…F interactions are significant at high pressure, there are none in the low-temperature form.

3.19. *Perfluorocyclopropene: experimental and theoretical studies of its structure in gaseous, solution, and crystalline phases*

A study on structure and bonding in perfluorinated compounds continues to attract interest and the smallest molecule of the perfluorocycloalkene class that has been studied is perfluorocyclobutene, C_4F_6. However the simplest member of the class is 1,2,3,3-tetrafluorocyclopropene, which is a toxic, flammable and explosive gas[23]. This compound is of particular interest as the ring strain leads to some unusual structural parameters. The large coupling constants for the C–F bond, symmetry, distribution of spin 1/2 nuclei and its volatility make it an ideal candidate for detailed structural study. The structure of 1,2,3,3-tetrafluorocyclopropene, C_3F_4, has been determined at 156 K by X-ray crystallography and in the gas phase by a combined analysis of electron-diffraction data, rotation constants derived from the microwave spectrum, and dipolar coupling constants derived from the liquid crystal ^{19}F NMR spectrum. The compound crystallizes in the orthorhombic centrosymmetric space group *Pbcn* (Figure 66(a)). Crystal structure is stabilized by C…F and F…F contacts. The analyses of both the electron diffraction and single crystal X-ray data are consistent with the spectroscopic evidence that the molecule consists of a three-membered ring consisting of C=C with the molecule having C_{2v} symmetry in gas phase and *C*2 symmetry in the solid state (Table 2). The bond lengths and bond angles obtained for the low temperature solid phase structure are in excellent agreement with those obtained in an *ab initio* study of the molecular geometry at the electron-correlated MP2/TZ2P level, the gas phase as anticipated for a rigid-ring structure. The dipole moment of C_3F_4 has been determined from Stark effect measurements to be 1.313(4) D. The molecules are ordered in linear chains of coplanar C_3 rings, in each chain along the dipole moment vector.

Table 1: Comparison of the principal geometrical parameters for C_3F_4

Parameter [a]	E/MW/LCNMR	X-ray	Ab-initio [b]
d (C1-C3)	1.461(3)	1.453(3)	1.465
d (C1-C2)	1.307(13)	1.296(4)	1.312
d (C3-F6)	1.361(4)	1.370(2)	1.356
d (C1-F4)	1.315(3)	1.312(2)	130.8
∠C1-C2-F5	149.9 (6)	150.4(9)	149.8
∠F6-C3-F7	105.4(5)	104.1(2)	105.8
∠C1-C2-C3	63.4(3)	63.5(1)	63.4

a: For atom numbering scheme see Fig. 26(a). b: MP2/TZ2P level of theoretical calculations.

3.20. *Crystal structures of natural products*

The group of Andrew Bond has been actively involved in the determination of the crystal structures of heterocyclic amines[24], terpenes[25] and hydrocarbons, which are liquids or low melting solids at low temperature. Some of the most important compounds are 2,3-lutidine (Figure 67), 2,5-lutidine (Figure 69), 2,6-lutidine (Figure 71), 3, 4-lutidine (Figure 73), (1S)-(-)-α-Pinene (Figure 75), (1S)-(-)-β-Pinene (Figure 76), γ-terpinene (Figure 77), 2-picoline (Figure 79), 3-picoline (Figure 80), α-methylstyrene, (1R)-(-)-Fenchone (Figure 81), 2,4,6-Collidine, isopropylcyclohexane and methylcyclopentane. Amongst the different isomeric lutidines, the 2,3-isomer crystallizes in centrosymmetric monoclinic *C*2/*c* ($Z' = 1/2$ with the crystallographic *diad* passing through the C2–C2A bond and hence the

structure is disordered. C–H...N intermolecular interactions forming molecular chains are present in the crystal lattice (Figure 68). In the 2,5-isomer it crystallizes in the triclinic P-1 ($Z' = 2$). C–H...N polar chains are arranged in a parallel manner forming polar sheets (Figure 70). These sheets in adjacent layers are arranged antiparallel to each other. The 2,6-isomer it crystallizes in the noncentrosymmetric orthorhombic space group *Fdd*2 with ($Z' = 1/2$) with the crystallographic diad passing through N1 and C4. C–H...N interactions along the diad axis (001) are parallel resulting in a polar arrangement of molecules in the crystal lattice (Figure 72). The methyl substituents at 2,6-positions prevent the adoption of edge-face geometry with the planes of pyridyl rings of molecules between adjacent chains remaining essentially planar. Finally in the 3,4-isomer it crystallizes in the centrosymmetric *C*2/*c* space group ($Z' = 4$) wherein C–H...N intermolecular dimers stabilize the crystal lattice (1S)-(-)- β-Pinene (Figure 74).

The liquid hydrocarbons, (1S)-(-)-α-Pinene, (1S)-(-)-β-Pinene crystallize in the non-centrosymmetric space group $P2_12_12_1$ with Z = 4. The crystal structure is stabilized by van der Waals interactions. γ-terpinene crystallizes in the centrosymmetric space group *Pnma*. The molecule lies on the mirror plane and packs in a herringbone arrangement (Figure 78). In α-methylstyrene, the molecule packs in centrosymmetric $P2_1/n$. The molecular being planar is stabilized in the crystal lattice by C–H...π intermolecular interactions. 3-Picoline crystallizes in the noncentrosymmetric point group $Pna2_1$ with Z = 4 and packs in the herringbone type of arrangement with no C–H...N intermolecular interactions present. The 2-isomer also crystallizes in the non-centrosymmetric space group $P2_12_12_1$ but unlike the 3-isomer there are C–H...N interactions present in the crystal lattice. (1R)-(-)-Fenchone crystallizes in non-centrosymmetric $P2_1$ with Z = 2 molecules in the unit cell.

3.21. In situ *cryocrystallization and charge density studies on ethylene glycol*

Intra-molecular hydrogen bonding in ethane-1, 2-diol is one of the many unicorns of chemistry in the sense meant by Frenking and Krapp (2007), representing "*...a mystical animal whose appearance is known to everybody although nobody has ever seen one...*" (Figure 82)[26]. The experimental evidence for claiming that there is an intra-molecular hydrogen bond O–H...O in ethane-1, 2-diol and that this stabilises the *gauche* conformation, relies heavily on the interpretation of a small red-shift in the vibrational stretching frequency for the 'bound' O–H group compared to the unbound O–H group[27–30]. The observed vapour-phase red-shift for ethane-1, 2-diol is ~33 cm^{-1} [31] and in dilute carbon tetrachloride solution 32 cm^{-1} [32]. Figure 83 and 84 highlight the ORTEP view and the packing diagram of the molecules depicting O–H...O and C–H...O intermolecular interactions.

In order to establish the claim whether intra H-bond exists, EG was crystallized *in situ* on the diffractometer and charge density data collected at 150 K.

It is quite clear from the experimental electron density maps of ethane-1, 2-diol in the crystal (Figure 69) that there is no evidence for the presence of a (3, -1) bond critical point (BCP) for a putative intra-molecular O–H...O interaction (Figure 85).

4. Conclusions

The above-mentioned studies clearly demonstrate the fact, that the nature of intra- and intermolecular interactions which evolve on crystallizing liquids are similar to the ones observed in the solid state. It is indeed noteworthy that the latest developments in the field of CCD detectors has allowed for the collection of charge density datasets on molecules which are liquids at room temperature and to evaluate the topological features associated with them. In this context, the importance of weak interactions involving organic fluorine is unraveled, highlighting the directional preferences leading to the formation of well-defined packing motifs in the crystalline lattice.

Acknowledgements

We thank the Department of Science and Technology for funding and also for data collection on the CCD facility provided under the DST-IRHPA scheme. Deepak thanks CSIR, India and IISc, India for Research Associateship. We thank Vijay Thiruvenkatam, S.J. Prathapa for collaboration in some of the work reported. We sincerely acknowledge Professors R. Boese, A. D. Bond, N. Winterton, D. Rankin, S. Parsons and P. Luger for their kind acceptance to reproduce several figures with permission with the journal authorities their research work.

Received 16 June 2007; revised 18 July 2007.

References

1. (a) Nussbaumer, M.; Boese, R. In *Correlations, Transformations, and Interactions in Organic Crystal Chemistry, IUCr Crystallography Sumposia, Vol 7*; Jones, W. D.; Katrusiak, A; Eds. Oxford, **1994**, 20; (b) http://www.ohcd-system.com. (c) Bond, A. *Chem. Commun.*, **2003**, 250.
2. Viswamitra, M. A. *J. Sci. Inst.*, **1962**, 39, 381.
3. Viswamitra, M. A.; Kannan, K. K. *J. Sci. Inst.*, **1962**, 39, 318.
4. (a) Boese, R.; Weiss, H. -C.; Bläser, D. *Angew. Chem. Int. Ed. Engl.*, **1999**, 38, 988. (b) Thalladi, V. R.; Boese, R. *New J. Chem.*, **2000**, 24, 579.
5. Bond, A. *Chem. Commun.*, **2002**, 1664.
6. Thalladi, V. R.; Weiss, H.-C.; Boese, R. *Angew. Chem. Int. Ed. Engl.*, **2000**, 39, 918.
7. Thalladi, V. R.; Boese, R.; Weiss, H.-C. *J. Am. Chem. Soc.*, **2000**, 122, 1186.
8. Thalladi, V. R.; Nusse, M.; Boese, R. *J. Am. Chem. Soc.*, **2000**, 122, 9227.

9. Bond, A. *CrystEngComm*. **2006**, 8, 333.
10. Boese, R.; Niederprum, N.; Blaser, D.; Maulitz, A.; Antipin, M.Y.; Mallinson, P. R. *J. Phys. Chem. B*, **1997**, 101, 5794.
11. Antipin, M.Y.; Boese, R.; Blaser, D.; Maulitz, A. *J. Am. Chem. Soc.*, **1997**, 119, 326.
12. Boese, R.; Antipin, M.Y.; Blaser, D.; Konstantin, A. L. *J. Phys. Chem. B*, **1998**, 102, 8654.
13. (a) Choudhury, A. R.; Wintherton, N.; Steiner, A.; Cooper, A. I.; Johnson, K. A. *J. Am. Chem. Soc.,* , **2005**, 127, 16792. (b) Choudhury, A. R.; Wintherton, N.; Steiner, A.; Cooper, A. I.; Johnson, K. A. *CrystEngComm.*, **2006**, 8, 742.
14. Choudhury, A. R.; Islam, K.; Kirchner, M. T.; Mehta, G.; Guru Row, T. N. *J. Am. Chem. Soc.,* , **2004**, 126, 12274.
15. Kirchner, M. T.; Boese, R.; Billups, E. W.; Norman, L. R. *J. Am. Chem. Soc.*, **2004**, 126, 9407.
16. Boese, R.; Kirchner, M. T.; Billups, W. E.; Norman, L. R. *Angew. Chem. Int. Ed. Engl.*, **2003**, 42, 1961.
17. Boese, R.; Boese, A. D.; Blaser, D.; Antipin, M. Y.; Ellern, A.; Seppelt, K. *Angew. Chem. Int. Ed. Engl.*, **1997**, 36, 1489.
18. Bach, A.; Lentz, D.; Luger, P.; Messerchimdt, M.; Olesch, C.; Patzschke, M. *Angew. Chem. Int. Ed. Engl.*, **2002**, 41, 296.
19. Thalladi, V. R.; Weiss, H-C. ; Bläser, D.; Boese, R.; Nangia, A.; Desiraju, G. R. *J. Am. Chem. Soc.*, **1998**, 120, 8702.
20. Chopra, D.; Thiruvenkatam, V.; Guru Row, T. N. *Cryst. Growth & Des.*, **2006**, 6, 843.
21. Chopra, D.; Thiruvenkatam, V.; Manjunath, S. G.; Guru Row, T. N. *Cryst. Growth & Des.*, **2007**, 6, 843.
22. Oswald, I. D.H.; Allan, D. R.; Motherwell, W. D. S.; Parsons, S. *Acta Cryst.*, **2005**, *B*61, 69.
23. Abdo, B. T.; Alberts, I. L.; Attfield, C. J.; Banks, R. E.; Blake, A. J.; Brain, P. T.; Cox, A. P.; Pulham, C. R.; Rankin, D. W. H.; Robertson, H. E.; Murtagh, V.; Heppeler, A.; Morrison, C. *J. Am. Chem. Soc.*, **1996**, 118, 209.
24. (a) Davis, J. E.; Bond, A. D. *Acta Crystallogr.*, **2002**, *E*58, o961. (b) Davis, J. E.; Bond, A. D. *Acta Crystallogr.*, **2002**, *E*58, o326. (c) (d) Davis, J. E.; Bond, A. D. *Acta Crystallogr.*, **2001**, *E*57, o1141. (e) Davis, J. E.; Bond, A. D.; Kirby, A. J. *Acta Crystallogr.*, **2001**, *E*57, o1242. (f) Davis, J. E.; Bond, A. D.; Kirby, A. J. *Acta Crystallogr.*, **2002**, *E*58, o328. (g) Davis, J. E.; Bond, A. D.; Kirby, A. J. *Acta Crystallogr.*, **2001**, *E*57, o1087. (h) Davis, J. E.; Bond, A. D.; Kirby, A. J. *Acta Crystallogr.*, **2002**, *E*57, o1089.
25. (a) Davis, J. E.; Bond, A. D. *Acta Crystallogr.*, **2002**, *E*58, o331. (b) Davis, J. E.; Bond, A. D. *Acta Crystallogr.*, **2001**, *E*57, o1039. (c) Davis, J. E.; Bond, A. D.; Kirby, A. J. *Acta Crystallogr.*, **2001**, *E*57, o1032. (d) Davis, J. E.; Bond, A. D.; Kirby, A. J. *Acta Crystallogr.*, **2001**, *E*57, o1034. (e) Davis, J. E.; Bond, A. D.; Kirby, A. J. *Acta Crystallogr.*, **2001**, *E*57, o1041.
26. Frenking, G.; Krapp, A. *J. Comp. Chem.* **2007**, 28, 15.
27. Renault, B.; Cloutet, E.; Cramail, H.; Tassaing, T.; Besnard, M., *J. Phys. Chem. A*, **2007**, 111, 4181.
28. (a) Howard, D. L.; Jørgensen, P.; Kjaergaard, H.G.; *J. Am. Chem. Soc.*, **2005**, 127, 17096. (b) Howard, D. L.; Kjaergaard, H. G. *J. Phys. Chem. A*, **2006**, 110, 10245.
29. Kuhn, L.P.; *J. Am. Chem. Soc.*, **1952**, 74, 2492; *ibid.* **1954**, 76, 4323; *ibid.* **1958**, 80, 5950; Kuhn, M.; Lüttke, W.; Mecke, R.; *Z. Anal. Chem.*, **1959**, 170, 106.
30. Bellamy, L. J. "The Infrared Spectra of Complex Molecules" 3rd ed., volume 1, **1975**, Chapman and Hall, London.
31. Buckley, P.; Giguère, P. A. *Can. J. Chem.*, **1967**, 45, 397.
32. Eliel, E.L.; "*Stereochemistry of Carbon Compounds*" McGraw-Hill, New York, **1962**, p. 131: "…ethylene glycol may exist in two distinct stable conformations…, the anti conformation and gauche conformation (of which there are two enantiomers). Only in the latter are the hydroxyl groups close enough together to give rise to an intra-molecular bond…";

Deepak Chopra is a Research Associate in the Department of Solid State and Structural Chemistry Unit, Indian Institute of Science and currently working with Prof. T. N. Guru Row. He has done his Bachelors in Science (2001) from Jadavpur University, Kolkata and completed his Masters in Science (2004) followed by a PhD degree (2007) at Indian Institute of Science under the supervision of Prof. T. N. Guru Row. His research interests involve crystal engineering, polymorphism, *in-situ* cryocrystallography and topological analysis of the electron densities in molecular crystals via high resolution X-ray diffraction.

T. N. Guru Row is Professor in the Department of Solid State and Structural Chemistry Unit, Indian Institute of Science. He received his Bachelors Degree in Science (1969) from Bangalore University, Masters Degree from the same University (1971) followed by his PhD degree from Indian Institute of Science (1976). He is in the Editorial Board for Materials Research Bulletin and Acta Crystallographica E and also an Associate Editor of Journal of Indian Institute of Science. His research interests are in the area of high resolution Powder Diffraction, Rietveld refinements, ab-initio structures, phase transitions, Guest-Host complexes, Crystal Engineering via Charge Density Analysis in Molecular crystals, Cryo-crystallography, Generation of polymorphs, Photocatalysis and Structure Property Correlations in solids.